Title

Characterization of Isolated Ga^{3+} Cations in Ga/H-MFI Prepared by Vapor-Phase Exchange of H-MFI Zeolite with GaCl3

Journal

ACS Catalysis, 8(7)

ISSN

2155-5435

Authors

Phadke, NM
Van Der Mynsbrugge, J
Mansoor, E
et al.

Publication Date

2018-07-06

DOI

10.1021/acscatal.8b01254

Peer reviewed

ACS Catalysis

Research Article

Cite This: ACS Catal. 2018, 8, 6106−6126

pubs.acs.org/acscatalysis

Characterization of Isolated Ga^{3+} Cations in Ga/H-MFI Prepared by Vapor-Phase Exchange of H-MFI Zeolite with $GaCl_3$

Neelay M. Phadke,[†] Jeroen Van der Mynsbrugge,[†] Erum Mansoor,[†] Andrew Bean Getsoian,[‡] Martin Head-Gordon,[§] and Alexis T. Bell*[,†]

[†]Department of Chemical and Biomolecular Engineering, University of California, Berkeley, California 94720, United States

[‡]Chemical Engineering Department, Ford Motor Company, Dearborn, Michigan 48121, United States

[§]Department of Chemistry, University of California, Berkeley, California 94720, United States

Supporting Information

ABSTRACT: Ga/H-MFI was prepared by vapor-phase reaction of $GaCl_3$ with Brønsted acid O−H groups in dehydrated H-MFI zeolite. The resulting $[GaCl_2]^+$ cations in the as-exchanged zeolite are treated in H_2 at 823 K to stoichiometrically remove Cl ligands and form $[GaH_2]^+$ cations. Subsequent oxidation in O_2 and characterization by IR spectroscopy and NH_3-temperature-programmed desorption (TPD) suggests that, for Ga/Al ratios ≤0.3, Ga^{3+} exists predominantly as $[Ga(OH)_2]^+$−H^+ cation pairs and to a lesser degree as $[Ga(OH)]^{2+}$ cations at low Ga/Al ratios (∼0.1); while both species are associated with proximate cation-exchange sites, calculated free energies of formation suggest that $[Ga(OH)]^{2+}$ cations are more stable on cation-exchange sites associated with NNN (next-nearest neighbor) framework Al atoms than on those associated with NNNN (next-next-nearest neighbor) framework Al atoms. Ga K-edge X-ray Absorption Near Edge Spectroscopy (XANES) measurements indicate that, under oxidizing conditions and for all Ga/Al ratios, all Ga species are in the +3 oxidation state and are tetrahedrally coordinated to 4 O atoms. Fourier analysis of Ga K-edge Extended X-ray Absorption Fine Structure (EXAFS) data supports the conclusion that Ga^{3+} is present predominantly as $[Ga(OH)_2]^+$ cations (or $[Ga(OH)_2]^+$−H^+ cation pairs). For Ga/Al ratios ≤0.3, wavelet analysis of EXAFS data provide evidence for backscattering from nearest neighboring O atoms and from next-nearest neighboring framework Al atoms. For Ga/Al > 0.3, backscattering from next-nearest neighboring Ga atoms is also evident, characteristic of GaO_x species. Upon reduction in H_2, the oxidized Ga^{3+} species produce $[Ga(OH)H]^+$−H^+ cation pairs, $[GaH_2]^+$−H^+ cation pairs, and $[GaH]^{2+}$ cations. Computed phase diagrams indicate that the thermodynamic stability of the reduced Ga^{3+} species depends sensitively on temperature, Al−Al interatomic distance, and H_2 and H_2O partial pressures. For Ga/Al ratios ≤0.2, it is concluded that $[GaH_2]^+$−H^+ cation pairs and $[GaH]^{2+}$ cations are the predominant species present in Ga/H-MFI reduced above 673 K in 10^5 Pa H_2 and in the absence of water vapor.

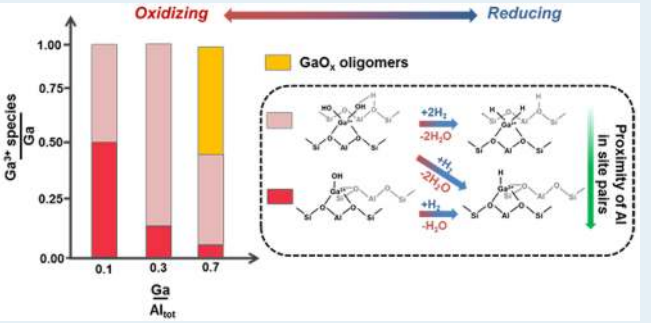

KEYWORDS: *gallium, cation-exchanged zeolites, vapor-phase ion exchange, X-ray absorption spectroscopy, heterogeneous catalysts, catalyst characterization, alkane dehydrogenation*

1. INTRODUCTION

The U.S. has large reserves of shale gas, much of which contains significant fractions of ethane and propane.[1] The availability of this relatively inexpensive source of light alkanes has stimulated the chemical industry to seek ways to use this resource for the production of olefins and aromatics via dehydrogenation and dehydrocyclization.[2] While Brønsted acid O−H groups in zeolites are capable of catalyzing both reactions, they also catalyze alkane and alkene cracking, thereby limiting the yields of alkenes and particularly aromatics.[3] In contrast, Ga, Zn, and Co-exchanged MFI zeolites have been found to be active and selective catalysts for the dehydrogenation and dehydrocyliza-tion of light alkanes.[4−6] To date, the most effective catalyst for the conversion of C_2−C_4 alkanes into olefins and aromatics has proven to be Ga/H-MFI, which is currently used in the Cyclar process.[7−9] For this reason, there has been considerable interest in understanding the nature of the Ga species present in Ga/H-MFI and understanding the role of these species in the dehydrogenation and dehydrocyclization of light alkanes.

A number of studies have focused on elucidating the structure of Ga cations ion-exchanged into H-MFI and their role in promoting C_3H_8 dehydrocyclization.[9−19] Nevertheless, the exchange stoichiometry, chemical structure, and molecularity of Ga species in Ga/H-MFI are not fully defined, in large part because of the way in which Ga/H-MFI is typically prepared. A conventional approach to introducing Ga cations

Received: April 1, 2018
Revised: May 16, 2018
Published: May 21, 2018

DOI: 10.1021/acscatal.8b01254
ACS Catal. 2018, 8, 6106−6126

into the MFI zeolite proceeds via incipient-wetness impregnation of H-MFI or NH_4-MFI with an aqueous solution of a Ga^{3+} salt, most commonly $Ga(NO_3)_3$, followed by calcination in O_2 at elevated temperatures in order to decompose the NO_3 ligands.[20,21] Ga/H-MFI prepared in this manner contains relatively little ion-exchanged Ga^{3+}, and a large fraction of the Ga deposits on the external surfaces of the zeolite crystal as crystalline GaO_x.[22] The reason for this is that hydrated Ga^{3+} cations undergo slow diffusion into the MFI channels due to steric and electronic repulsion, resulting in low levels of Ga^{3+} ion exchange.[22,23] Ion exchange between Brønsted acid O−H groups and Ga species has been observed to occur when Ga/H-MFI prepared by this means is reduced in H_2 or treated with gas-phase alkanes at temperatures >700 K.[10,14] It has been proposed that cation exchange occurs via reduction of GaO_x agglomerates to form volatile Ga_2O monomers, which migrate into the MFI channels and react with Brønsted acid O−H groups to form Ga^+ or GaH_x cations.[20,22−24] It is notable that, even after H_2 reduction, Ga/H-MFI is found to contain detectable amounts of crystalline GaO_x.[22] As a result of the nonuniform state of Ga species (either as exchanged cations or neutral GaO_x) in conventionally prepared Ga/H-MFI, elucidation of the structure of the active form of exchanged Ga cations has proven to be challenging.[25]

Attempts have been made to prepare isolated Ga cations in H-MFI by means other than wet impregnation with $Ga(NO_3)_3$. Kwak and Sachtler have synthesized Ga/H-MFI by vapor-phase reaction of Brønsted acid O−H groups with $GaCl_3$.[15] However, these authors did not provide conclusive evidence for $GaCl_3$ grafting, removal of residual Cl ligands, and the chemical structure of the Ga^{3+} cations existing in the as-prepared materials. García-Sánchez and co-workers and Rane et al. have synthesized Ga/H-MFI by grafting Ga^{3+} at cation-exchange positions in the zeolite via reaction of $Ga(CH_3)_3$ with Brønsted acid O−H groups.[12,26] This volatile precursor was found to react unselectively with both Brønsted acid O−H and Si−OH groups. While complete titration of Brønsted acid O−H groups in the zeolite with Ga^{3+} cations could be achieved (i.e., Ga/Al = 1), no attempts were made to systematically examine the effects of Ga/Al ratio on the structure of the grafted Ga^{3+} cations.[26]

The aim of the present work was to produce isolated Ga^{3+} species in Ga/H-MFI with Ga/Al ratios of 0.1 to 0.7. This objective was achieved via the reaction of Brønsted acid O−H groups in H-MFI with $GaCl_3$ vapor. By carefully controlling synthesis parameters and employing detailed chemical and spectroscopic probes in combination with theoretical calculations, we were able to demonstrate that, in the oxidized state and for Ga/Al ratios ≤0.3, Ga/H-MFI contains predominantly isolated $[Ga(OH)_2]^+$ cations, present as $[Ga(OH)_2]^+$−H^+ cation pairs, and a small fraction of divalent $[Ga(OH)]^{2+}$ cations. Both cationic species are associated with proximate cation-exchange sites associated with pairs of framework Al atoms. Experimental determination of the Ga^{3+} exchange stoichiometry in concert with theoretical calculations suggests that, at low Ga/Al ratios (~0.1), $[Ga(OH)]^{2+}$ cations form at proximate cation-exchange sites for which the Al−Al distances are ≤5 Å, whereas $[Ga(OH)_2]^+$−H^+ cation pairs form at proximate cation-exchange sites for which the framework Al atoms are farther apart. The concentration of the latter structure increases with increasing Ga content until all available proximate cation-exchange sites are saturated at a Ga/Al ratio of ~0.3. For higher Ga/Al ratios, introduction of additional Ga results in the formation of GaO_x oligomers. Upon H_2 reduction of as-prepared Ga/H-MFI, both $[Ga(OH)]^{2+}$ cations and $[Ga(OH)_2]^+$−H^+ cation pairs convert into $[Ga(OH)H]^+$−H^+ cation pairs. For proximate cation-exchange sites with sufficiently short interatomic framework Al−Al distances (≤5 Å) at low Ga/Al ratios, $[Ga(OH)H]^+$ cations may undergo condensation with proximate Brønsted acid O−H groups to form $[GaH]^{2+}$ cations. Theoretically determined phase diagrams of Ga^{3+} hydride structures suggest that the nature of Ga^{3+} species formed upon H_2 reduction is highly sensitive to the framework Al−Al interatomic distance in proximate cation-exchange sites and to the relative partial pressures of H_2O and H_2. Under sufficiently anhydrous reducing conditions (≤10^{-1} Pa H_2O, >10^3 Pa H_2), $[Ga(OH)H]^+$−H^+ cation pairs may further reduce to $[GaH_2]^+$−H^+ cation pairs. At temperatures above 713 K, $[GaH_2]^+$ cations undergo a change in coordination from 4 to 3, with a reduction in the number of framework Ga−O_f bonds from 2 to 1.

2. EXPERIMENTAL AND THEORETICAL METHODS

2.1. Synthesis of Ga/H-MFI Catalysts. The parent H-MFI sample was prepared by heating 1−2 g batches of NH_4-MFI (Zeolyst, CBV 3024E) in quartz boats placed in a tubular quartz tube, at 2 K min^{-1} from ambient temperature to 773 K in flowing synthetic dry air (Praxair, ultra zero, 100 mL min^{-1}). Samples were held at 773 K for 4 h to convert the NH_4 form of the zeolite into the H form. The bulk Si/Al ratio of the zeolite was determined to be 16.5 ± 1.0 by ICP-OES carried out by Galbraith Laboratories (Knoxville, TN). Previous work (using Co^{2+} cation titration) in our group has shown that the fraction of proximate cation-exchange sites associated with pairs of framework Al atoms present as either next-nearest neighbor (NNN) or next-next-nearest neighbor (NNNN) is approximately 45% of the framework Al.[27]

Prior to carrying out the vapor-phase exchange with $GaCl_3$, H-MFI was dehydrated by placing 2 g of the zeolite in a 20 mL glass ampule and heating it to 573 K in a sand bath for 3 h under dynamic vacuum using a Schlenk line. The dehydrated H-MFI was sealed and then transferred into a N_2-purged glovebox. This material was intimately mixed with anhydrous $GaCl_3$ (99.999% Strem chemicals) in a porcelain crucible inside the glovebox, to achieve Ga/Al ratios of 0.1 to 0.7. Each physical mixture was then loaded into a fresh glass ampule and taken out of the glovebox, sealed under N_2. Samples were cooled by immersing in a liquid N_2 bath, to prevent loss of Ga content due to evaporation of $GaCl_3$. The ampule was then evacuated and flame-sealed under dynamic vacuum, heated in a furnace at 5 K min^{-1} to 478 K, and held at this temperature for 2 h before being cooled to ambient temperature. This procedure led to sublimation of $GaCl_3$ and reaction of gas-phase $GaCl_3$ with Brønsted acid O−H groups in the zeolite. Following the sublimation step, the contents of the ampule were transferred to quartz boats (1−2 g) and heated in a tubular quartz tube under flowing dry synthetic air (Praxair, ultra zero, 100 mL min^{-1}) at 2 K min^{-1} to 773 K, held for 1 h, and then cooled to 363 K. The system was flushed with He for 5 min, and the flow was then switched to 10^5 Pa H_2 (Praxair, 100 mL min^{-1}). Samples were heated under H_2 flow at 5 K min^{-1} to 823 K, held at this temperature for 2 h, and then cooled to 623 K. At this temperature, the system was flushed with pure He for 10 min after which flow was switched back to dry synthetic air (Praxair, ultra zero, 100 mL min^{-1}). Samples were heated under flowing air at 5 K min^{-1} to 773 K, held for 1 h, and then cooled to ambient temperature. This procedure was

DOI: 10.1021/acscatal.8b01254
ACS Catal. 2018, 8, 6106−6126

required to convert grafted $[GaCl_2]^+$ to $[GaH_2]^+$ cations and to oxidize the latter species to $[Ga(OH)_2]^+$ cations. The effluent from these reduction/oxidation treatments was passed through an $H_2O/NaHCO_3$ trap in order to trap any HCl released. Ga/H-MFI samples were stored in a glovebox until further use. Chloride titration was performed on the contents of the $H_2O/NaHCO_3$ trap (attached to the outlet line from the synthesis reactor) in order to quantify the HCl released during reduction/oxidation treatments of grafted samples. These titrations were performed using Mohr's method: $NaHCO_3$ was added to the solution until it reached a neutral pH. The resulting solution was then titrated against $Ag(NO_3)_3$ using K_2CrO_4 as an indicator in order to directly estimate Cl concentrations.[28] Ga/Al ratios and Cl/Ga ratios of Ga/H-MFI samples (post reduction/oxidation treatments) were determined by ICP-OES at Galbraith Laboratories.

2.2. Chemical and Spectroscopic Characterization of Ga/H-MFI Samples. Raman spectra of Ga/H-MFI samples were acquired using a LabRam HR Horiba Jobin Yvon Raman spectrometer with a 532 nm C.W. 50 mW laser. Samples of Ga/H-MFI (~100 mg) were loaded into an in situ Raman cell equipped with a quartz window (Linkam stage, CCR1000) and heated under flowing dry air (Praxair, extra dry, 100 mL min^{-1}) from ambient temperatures at 5 K min^{-1} to 1023 K, held at this temperature for 0.5 h, and then cooled to ambient temperature. Raman spectra of β-Ga_2O_3 (Sigma-Aldrich) were acquired at ambient temperature. An average of three Raman scans was recorded per measurement. Raman spectra were normalized to the band at 800 cm^{-1} characteristic of T-O-T vibrations of the zeolite framework.[29]

Infrared spectra of H-MFI and Ga/H-MFI samples were acquired in transmission mode using a Nicolet 670 FTIR spectrometer. Samples (~30 mg) were pressed into thin wafers and transferred into a cylindrical stainless steel sample holder. The sample and sample holder were sealed in a low dead-volume, in situ infrared cell equipped with CaF_2 windows. Prior to the acquisition of spectra, all samples were heated under flowing dry synthetic air (Praxair, ultra zero, 100 mL min^{-1}) at 2 K min^{-1} to 773 K, held for 0.5 h, and then cooled to 723 K. Spectra were collected at 723 K by averaging 64 scans with a resolution of 2 cm^{-1}. In order to examine the effects of H_2 treatment, calcined samples were exposed to 3% H_2/He (Praxair, 75 mL min^{-1}) at 773 K and treated for 1 h at this temperature. Samples were then cooled to 473 K for measurement. All infrared spectra were baseline corrected (using a Spline function) and normalized to the intensity of Si−O−Si framework overtone bands occurring between 1700 and 2000 cm^{-1}. The fraction of Brønsted acid O−H groups exchanged by Ga^{3+} at each Ga/Al ratio was determined by integrating the area of the infrared band of Brønsted acid O−H stretching vibrations at 3593 cm^{-1} for each Ga/Al ratio and then normalizing this area by the area of this band in the parent H-MFI sample, as shown in the equation below.

$$\text{fraction of Brønsted } H^+ \text{ exchanged per total } H^+ = 1 - \frac{\text{integrated area of } 3593\ cm^{-1} \text{ band, Ga/H-MFI}}{\text{integrated area of } 3593\ cm^{-1} \text{ band, H-MFI}} \quad (1)$$

NH_3-temperature-programmed desorption (TPD) profiles of H-MFI and Ga/H-MFI samples were measured using a home-built apparatus. Samples (~0.2 g) were placed on a quartz wool plug inside a tubular quartz reactor (~0.6 cm sample bed height) with a thermocouple placed directly above the catalyst bed. Samples were treated under flowing dry synthetic air (Praxair, ultra zero) at a flow rate of 100 mL min^{-1}, heated at 5 K min^{-1} from ambient temperature to 773 K, and held at this temperature for 0.3 h. The reactor was then cooled to 433 K upon which the flow to the samples was switched to a gas mixture consisting of 1.7% NH_3 (Praxair, 99.9%) diluted in He (Praxair, UHP) at a flow rate of 305 mL min^{-1}. The samples were exposed to this gas mixture for 1 h in order to saturate Brønsted acid O−H groups with NH_3. The specific saturation temperature was chosen to minimize NH_3 adsorption at Lewis acid centers since the maximum rate of NH_3 desorption from Lewis acid sites in H-MFI was found to occur at 433 K. After completion of the saturation step, samples (at 433 K) were flushed in 300 mL min^{-1} He (Praxair, UHP) for 0.2 h. This step was followed by a treatment of the sample (held at 433 K) in 1% H_2O diluted in He (Praxair, UHP) at a flow rate of 300 mL min^{-1} for a period of 8 h. H_2O was introduced into the system via a syringe pump (Cole-Parmer) at a flow rate of 0.13 mL/h. This treatment was found to be necessary to remove NH_3 bound to Lewis acid centers in samples. Samples (held at 433 K) were then purged in dry He (Praxair, He) at a flow rate of 300 mL min^{-1} for 4 h before being cooled to 323 K. NH_3-TPD profiles were measured by heating samples at 5 K min^{-1} from 323 to 673 K under a gas mixture consisting of 1% Ar (Praxair, CSG) diluted in He (Praxair, UHP) at a flow rate of 300 mL min^{-1}. A capillary connected directly below the sample carried the reactor effluent into a mass spectrometer (MKS, Cirrus) and was used to quantify the desorbed NH_3. The NH_3 response factor was calibrated using mixtures of NH_3 and He. Ar was used as an internal standard to correct for drift in the NH_3 response factor. NH_3-TPD measurements on H_2-treated Ga/H-MFI samples were conducted after NH_3-TPD measurements on the same oxidized Ga/H-MFI samples. After an initial NH_3-TPD measurement, samples at 823 K were exposed to 5% H_2/He at a total flow rate of 300 mL min^{-1}, for a duration of 1 h. For both oxidized and reduced Ga/H-MFI samples, the remaining steps in the experimental protocol were identical. The fraction of Brønsted acid O−H groups exchanged by Ga^{3+} species was estimated from eq 2 and measured values of NH_3/Al_{tot} for H-MFI and Ga/H-MFI assuming a 1:1 stoichiometry between desorbed NH_3 and Brønsted acid O−H groups.

$$\text{fraction of } H^+ \text{ sites exchanged per total } H^+ = 1 - \frac{NH_3/Al_{tot},\ \text{Ga/H-MFI}}{NH_3/Al_{tot},\ \text{H-MFI}} \quad (2)$$

^{29}Si MAS and ^{27}Al MAS NMR spectra were acquired at the NMR facility at the University of California, Davis, on a 500 MHz NMR spectrometer. Samples (~300 mg) were hydrated in a desiccator containing H_2O for 24 h prior to measurement. Samples were then loaded into ZrO_2 rotors. All ^{29}Si MAS NMR spectra were collecting using a 7 mm probe at a spinning frequency of 6 kHz with a pulse length of 1.9 μs (corresponding to a 45° tip angle) and a relaxation delay time of 30 s. Spectra were referenced to tetramethylsilane (TMS) for which the isotropic chemical shift was set to 0 ppm. Framework Si/Al_f ratios were determined from ^{29}Si MAS NMR spectra by integrating the areas of bands obtained by spectral deconvolution.[30] All ^{27}Al MAS NMR spectra were collected using a 2.5 mm probe spinning at a frequency of 25 kHz with a pulse length of 0.23 μs (corresponding to a 30° tip angle) and a relaxation delay time of 0.2 s. The final spectra were obtained

DOI: 10.1021/acscatal.8b01254
ACS Catal. 2018, 8, 6106−6126

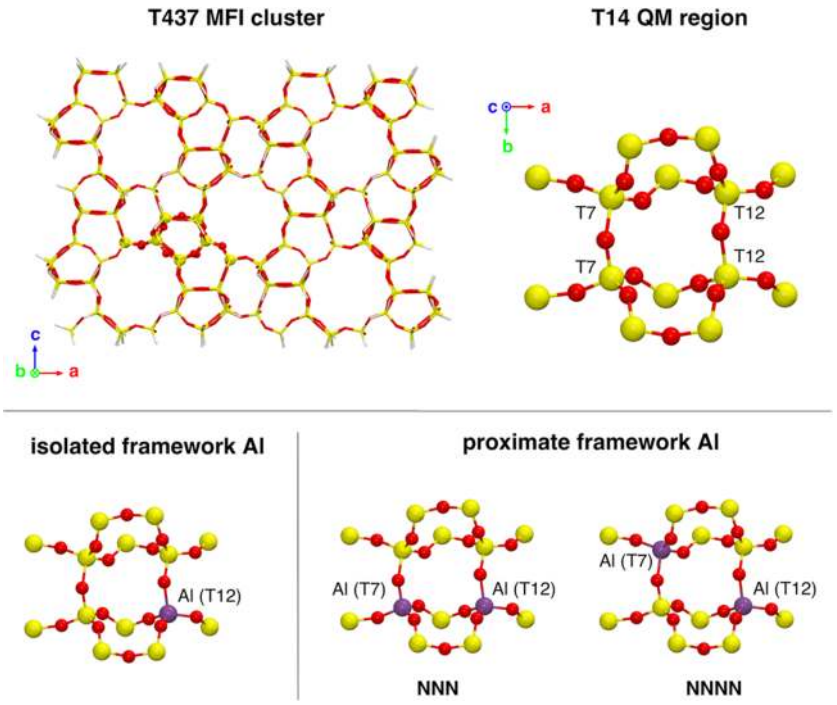

Figure 1. (Top left) T437 MFI cluster model used for QM/MM calculations, with T14 QM region shown in ball-and-stick representation. (Top right) Close-up of T14 QM region, with indication of T sites considered for Al substitution (T7 and T12). (Bottom left) Location of isolated framework Al in T14 QM region. (Bottom right) Location of proximate framework Al atoms in next-nearest neighboring (NNN) or next-next-nearest neighboring (NNNN) configuration in T14 QM region.

by averaging 8192 scans. Spectra were referenced with respect to aqueous $Al(NO_3)_3$ for which the isotropic chemical shift was set to 0 ppm. Tetrahedral framework Al centers in zeolites show a chemical shift of roughly 56 ppm relative to aq. $Al(NO_3)_3$ while octahedral Al centers in zeolites show no shift relative to aq. Al $(NO_3)_3$, i.e., a chemical shift of 0 ppm.[31] The relative fraction of tetrahedral and octahedral Al centers was determined by integrating the areas under spectral bands.

Ga K-edge X-ray absorption spectroscopy (XAS) data were acquired at beamline 5BMD at the Argonne Photon Source (APS). The monochromator energy was calibrated using β-Ga_2O_3, and all measurements were conducted in transmission mode. All edge energies were referenced to β-Ga_2O_3 for which the edge energy was set to 10375.1 eV. β-Ga_2O_3 standards β-Ga_2O_3 (Sigma-Aldrich) and $Ga(acac)_3$ (Strem chemicals) were sealed inside Kapton tape for measurements. Ga/H-MFI samples (~10 mg) were pressed into self-supporting pellets and placed inside a stainless steel 6-shooter sample holder. The sample holder was placed inside a quartz tube with a gas inlet and outlet and sealed at two ends with Kapton windows. The quartz tube was fitted inside a clam-shell furnace connected to a heater and temperature controller. Gases were metered to the in situ cell via mass flow controllers. XAS measurements were acquired on samples in their hydrated state at ambient conditions, upon calcination in 20% O_2/He (Airgas, 100 mL min^{-1}) to 773 K and upon treatment in 3% H_2/He (Airgas, 100 mL min^{-1}) at 603 K, 713 K, and 823 K. Both X-ray absorption Near Edge Structure (XANES) and Extended X-ray Absorption Fine Structure (EXAFS) measurements were made at the Ga K-edge. X-ray absorption spectra were background-corrected and normalized using the Athena software.[32] Ga K-edge energies were defined by the lowest energy inflection point in the edge region of the first derivative of the XAS spectrum. EXAFS spectra were Fourier transformed and fitted to the first coordination shell using the Artemis software,[32] and amplitude and phase shift scattering functions were calculated using the crystal structure of $CaGa_2O_4$[33] in Artemis via FEFF6, while values for the amplitude reduction factor S_0^2 were obtained by fitting the first coordination shell of the EXAFS spectra of β-Ga_2O_3. Wavelet transforms of EXAFS spectra were obtained by using the k^2-weighted EXAFS signal ($k^2\chi(k)$) as an input to the HAMA software,[34] and wavelet contour plots were prepared using OriginPro 2017.

H_2-temperature-programmed reduction (TPR) profiles were measured using a home-built apparatus. Samples (~0.18 g) were supported on a quartz wool plug placed inside a tubular quartz reactor with a thermocouple placed above the catalyst bed. Under 100 mL min^{-1} dry synthetic air (Praxair, ultra zero), samples were heated at 5 K min^{-1} to 773 K and held at this temperature for 1 h, before being cooled to 323 K. H_2-TPR profiles were measured by heating samples at 10 K min^{-1} from 323 to 1023 K under a flowing gas mixture of 1% H_2, 1% Ar diluted in He (Praxair, CSG) at a flow rate of 30 mL min^{-1}. A capillary placed directly below the sample carried the reactor effluent to a mass spectrometer (MKS, Cirrus). The response factor for H_2O was determined by flowing mixtures of H_2O (introduced into the system via syringe pump) diluted in He (UHP). The Ar in the gas mixture was used as internal standard to correct for drift in the H_2O mass spectrometer response factor.

2.3. Theoretical Calculations. All structures proposed for the isolated Ga^{3+} species were modeled using a hybrid quantum mechanics/molecular mechanics (QM/MM) method[35,36] applied to a large cluster model of MFI containing 437 tetrahedral atoms (T437), shown in Figure 1. A T14 cluster containing a distorted 6-ring at the intersection of the straight and sinusoidal channel and two adjacent 5-rings was treated quantum mechanically with the dispersion-corrected ωB97X-

DOI: 10.1021/acscatal.8b01254
ACS Catal. 2018, 8, 6106−6126

Scheme 1. Grafting of $[Ga(OH)_x]^{(3-x)+}$ (x = 1, 2) Cations at Isolated and Proximate Cation-Exchange Sites in Ga/H-MFI via $GaCl_3$ Vapor-Phase Exchange[a]

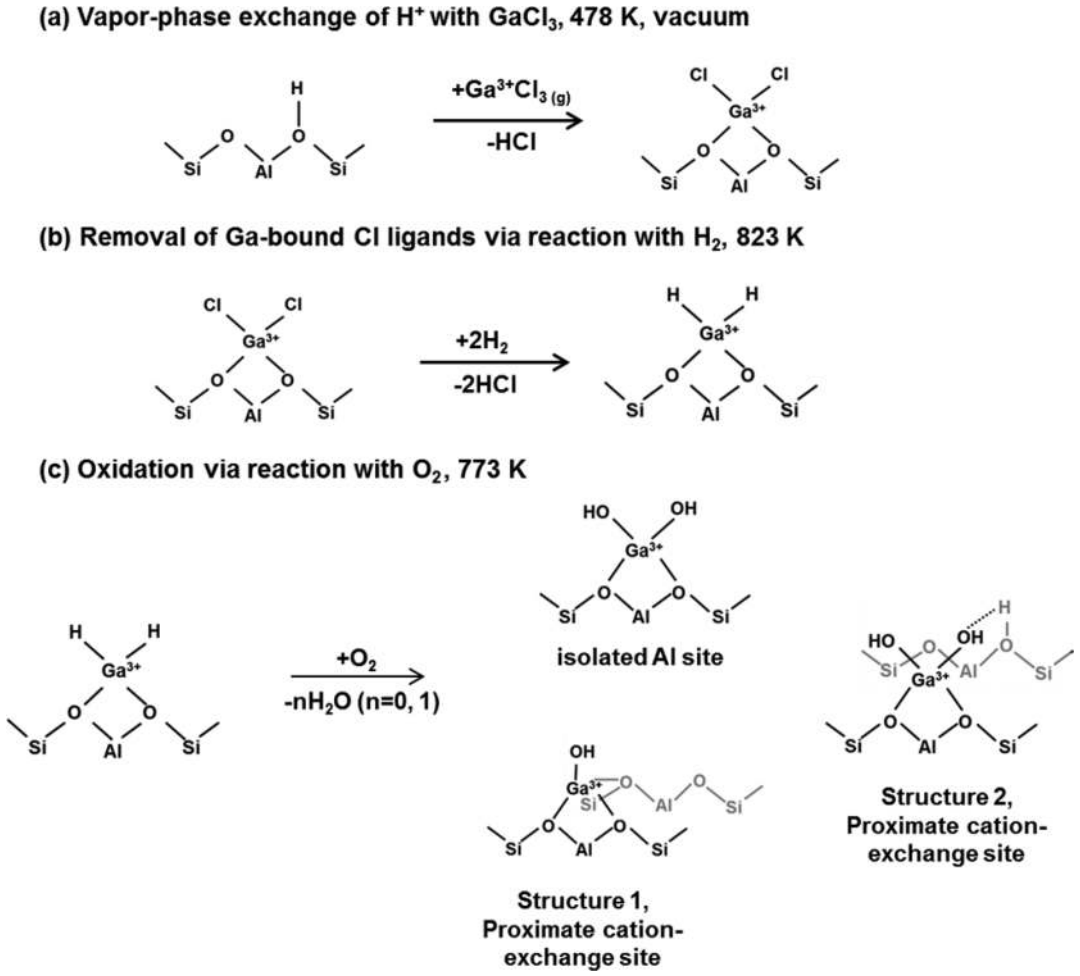

[a](a) Grafting of $GaCl_3$ at cation-exchange sites at 478 K under vacuum. (b) Removal of Cl ligands via reaction with H_2, at 823 K and 10^5 Pa H_2 (100 mL min^{-1}). (c) Oxidation of GaH_x cations to $[Ga(OH)_x]^{(3-x)+}$ (x = 1, 2) cations.

D[37,38] functional, while the remainder of the framework was described with molecular mechanics parameters taken from previous work (P2 parameter set).[36]

Both univalent and divalent site structures were investigated. The univalent site structures (e.g., $[Ga(OH)_2]^+$and $[GaH_2]^+$) compensate for the charge associated with an isolated Al atom in the MFI framework. The Al atom associated with these sites was placed in a T12 crystallographic position, which is located at the intersection of the straight and sinusoidal channels. This location is commonly selected for Al substitution in theoretical studies on H-MFI.[39−45] On the other hand, oxidized divalent cations, $[Ga(OH)]^{2+}$ and $[Ga(OH)_2]^+$−H^+ cation pairs, and reduced divalent cations, $[GaH]^{2+}$ and $[Ga(OH)H]^+$−H^+ and $[GaH_2]^+$−H^+ cation pairs, are compensated by proximate cation-exchange sites associated with pairs of framework Al atoms. Two cases with different Al−Al distances were examined: a next-nearest neighbor (NNN) pair, in which the two framework Al atoms are separated by one framework Si atom, and a next−next nearest neighbor (NNNN) pair, in which the two framework Al atoms are separated by two framework Si atoms. To create the pair sites, an additional Al atom was inserted in an NNN or NNNN T7 position relative to the T12 position (see Figure 1). This particular NNNN configuration was found to be relevant in earlier theoretical work[46] for ethane dehydrogenation catalyzed on $[GaH]^{2+}$ structures in Ga/H-MFI.

Initial geometries were constructed with ZEOBUILDER.[47] Geometry optimizations and frequency calculations were performed using the ωB97X-D/6-31G(d,p) level of theory for the QM region. Subsequent energy refinements on the stationary points were calculated at the ωB97X-D/6-311++G(3df,3pd) level. All QM/MM calculations were performed with a developmental version of Q-Chem.[48] Gibbs free energies at reaction temperatures (773 K for oxidized structures and 673 K for reduced structures) were derived from a normal-mode analysis using the quasi-rigid rotor/harmonic oscillator approximation[36,49] on the various stationary points obtained from QM/MM. Phase diagrams for oxidized and H_2-treated Ga^{3+} structures located at proximate cation-exchange sites associated with NNN and NNNN pairs of framework Al atoms were constructed by comparing the free energy of formation for various candidate structures starting from $[Ga(OH)_2]^+$−H^+ cation pairs and plotting the regions in which specific structures exhibit the lowest free energy of formation as a function of temperature and H_2 partial pressure at a given H_2O partial pressure. The following equations were used to determine the free energy of formation of specific Ga^{3+} structures from $[Ga(OH)_2]^+$−H^+ cation pairs.

DOI: 10.1021/acscatal.8b01254
ACS Catal. 2018, 8, 6106−6126

$$[Ga(OH)_2]^+ - H^+ + (x-2)H_2O + \left(2 - x + \frac{y-3}{2}\right) H_2 \rightarrow [GaO_xH_y]^{2+} \quad (3)$$

$$\Delta G_{form} = \Delta G_{[GaO_xH_y]^{2+}} - \Delta G_{[Ga(OH)_2]^+ - H^+} - (x-2)(\Delta G_{H_2O} - \Delta G_{H_2}) - \left(\frac{y-3}{2}\right)\Delta G_{H_2} \quad (4)$$

3. RESULTS AND DISCUSSION

3.1. Characterization of Ga/H-MFI Prepared by Treatment of H-MFI with $GaCl_3$ Vapor and Subsequent Removal of Ga-Bound Cl by H_2 Reduction. When physical mixtures of anhydrous H-MFI and $GaCl_3$ are heated to 478 K under vacuum, vapor-phase ion exchange occurs via the reaction of gas-phase $GaCl_3$ monomers or Ga_2Cl_6 dimers[50] with Brønsted acid O−H groups associated with framework Al sites located inside the channels of H-MFI. This reaction, shown in Scheme 1, is assumed to result in the grafting of $GaCl_3$ at cation-exchange sites associated with isolated framework Al atoms to form monovalent $[GaCl_2]^+$ cations or at proximate cation-exchange sites associated with pairs of framework Al atoms, either NNN (next-nearest neighbor) or NNNN (next-next-nearest neighbor), to form either divalent $[GaCl]^{2+}$ cations or monovalent $[GaCl_2]^+$ cations. Reduction of the grafted samples in flowing 10^5 Pa H_2 at 823 K resulted in near complete removal (>95% of Cl initially present; see Table S.1) of the Cl associated with Ga^{3+} species. Table 1 lists the

Table 1. Elemental Composition of Ga/H-MFI (Ga/Al Ratios) and HCl/Ga Ratios Derived by Quantifying HCl Desorbed during H_2 Treatment of $GaCl_x$/H-MFI at 10^5 Pa H_2 and 823 K

sample	HCl/Ga[c]
H-MFI[a]	–
Ga/Al[b]	–
0.1	1.5
0.2	1.6
0.3	1.8
0.4	2.2
0.5	1.6
0.7	1.7

[a]H-MFI, Zeolyst Batch CBV3024E, Si/Al_{tot} = 16.5 ± 1.0 (ICP-OES, Galbraith Laboratories). [b]Elemental compositions determined by ICP-OES (Galbraith Laboratories). [c]HCl/Ga ratios determined via Mohr's Cl titration protocol[28] on effluent collected in the $H_2O/NaHCO_3$ trap during H_2 treatment of $GaCl_x$-MFI samples at 823 K.

composition of Ga/H-MFI samples prepared with Ga/Al ratios of 0.1 to 0.7. Attempts to synthesize samples with Ga/Al > 0.7 were unsuccessful; loss of Ga from such samples was observed during H_2 reduction, presumably due to removal of Ga^{3+} as gas-phase $GaHCl_x$[51] (see Text S.1). HCl generated as a result of H_2 treatment was collected in an H_2O trap and quantified via chloride titration. HCl/Ga ratios determined by this means, shown in Table 1, ranged from 1.5 to 2.2 (with an average HCl/Ga = 1.7 ± 0.5). This stoichiometry suggests the grafting of $GaCl_3$ predominantly produces $[GaCl_2]^+$ cations, as suggested in Scheme 1. Since most of the Cl in these cations is removed during H_2 reduction, we propose that the $[GaH_2]^+$ cations form as a result of this treatment. Evidence for $[GaH_2]^+$ cations was obtained from in situ infrared spectra of reduced $GaCl_x$/H-MFI, which showed the presence of an infrared band at 2051 cm^{-1} which was absent in the infrared spectra of H-MFI upon H_2 treatment (see Figure S.1). This band is assigned to Ga−H stretching vibrations, consistent with previous experimental and theoretical studies.[52−54]

3.2. Characterization of As-Prepared Ga/H-MFI Following Oxidation. Following H_2 reduction of as-exchanged Ga/H-MFI, samples were oxidized in 2.0×10^4 Pa of O_2 at 773 K for 1 h in order to form air-stable Ga^{3+} hydroxide species, as shown in Scheme 1. The resulting materials showed no evidence for the formation of crystalline β-Ga_2O_3 in Raman spectra of even the highest Ga/Al ratios synthesized (Ga/Al = 0.5, 0.7) (see Text S.2 and Figure S.2). Oxidized Ga/H-MFI samples were characterized in order to determine the fraction of Brønsted acid O−H groups that were ion-exchanged and the exchange stoichiometry of the resulting Ga^{3+} cations. The local chemical environment around Ga^{3+} centers was then characterized by Ga K-edge X-ray absorption spectroscopy (XANES and EXAFS). Theoretical calculations were performed in order to evaluate the stability of candidate Ga^{3+} structures on isolated cation-exchange sites and on proximate cation-exchange sites associated with NNN and NNNN pairs of framework Al atoms.

Infrared spectroscopy and temperature-programmed desorption of NH_3 (NH_3-TPD) were used to probe the fraction of Brønsted acid O−H groups in oxidized Ga/H-MFI exchanged by Ga^{3+} and the exchange stoichiometry of the resulting Ga^{3+} cations. Figure 2a shows the infrared spectra of H-MFI and Ga/H-MFI samples measured under oxidizing conditions at 723 K. All spectra show a band at ∼3593 cm^{-1} attributable to ν(O−H) of Brønsted acid O−H groups[55] and a band at ∼3740 cm^{-1} attributable to ν(O−H) of Si−OH groups, located at defect sites inside the zeolite pores or at the external surfaces of the zeolite crystals.[56] As the Ga content in the samples increases, the area of the band at 3593 cm^{-1} decreases monotonically up to a Ga/Al ratio of ∼0.3, suggesting that Ga^{3+} species replace Brønsted acid O−H groups in these samples. For samples with Ga/Al ratios >0.3, the band at 3740 cm^{-1} decreases slightly in area (<30%), suggesting that $GaCl_3$ may also have reacted with less acidic Si−OH groups.

The infrared spectra of all Ga/H-MFI samples also show a weak band at 3660 cm^{-1}, absent in the infrared spectra of H-MFI. This band has been attributed previously to Al−OH groups in extra-framework Al (EFAl) species[57] or to OH groups coordinated to extra-framework cations (for example, $[Cu(OH)]^+$ cations in Cu-exchanged zeolites).[13,58] Contact with $GaCl_{3(g)}$ during vapor-phase exchange and with $HCl_{(g)}$ during Cl removal treatments could, in principle, lead to the extraction of framework Al and the concomitant formation of EFAl, in a manner similar to that reported for zeolites treated with $SiCl_4$ vapor at elevated temperatures.[59] Na exchange[27] and NH_3-TPD (discussed below) reveal that our parent H-MFI sample contains approximately 13−15% EFAl. Framework Si/Al_f ratios, estimated via deconvolution of ^{29}Si MAS NMR spectra (see Figure S.4) for H-MFI (Si/Al_f = 16.8) were similar within 10−15% uncertainty to Si/Al_f values for Ga/H-MFI (14.4−17.7) and to Si/Al_{tot} values from elemental analysis (16.5 ± 1.0) (see Table S.2). In addition, no discernible trend was observed in Si/Al_f values as a function of Ga content. As discussed in the Text S.3, these data suggest that the fraction of EFAl is similar in H-MFI and in Ga/H-MFI samples. As a consequence, we infer that the band at 3660 cm^{-1} in the

DOI: 10.1021/acscatal.8b01254
ACS Catal. 2018, 8, 6106−6126

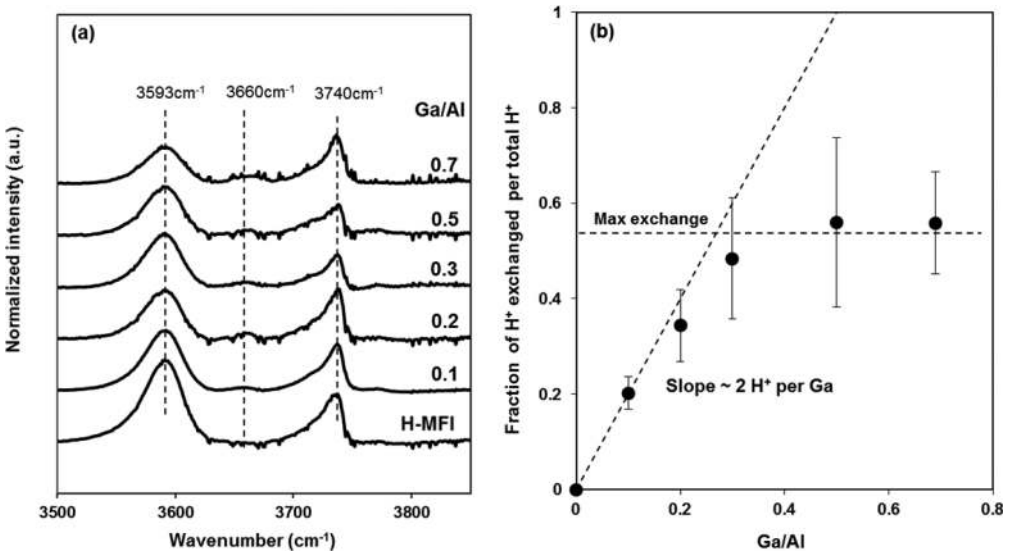

Figure 2. (a) Infrared spectra of H-MFI and Ga-MFI samples with Ga/Al ranging from 0.1 to 0.7. Infrared spectra were collected at 723 K under flowing dry air. (b) Fraction of H^+ (Brønsted O−H) exchanged per H_{total}^+ determined from infrared spectra, as a function of Ga/Al ratio. Dotted lines indicate slope of plot and maximum extent of H^+ exchange. Reported uncertainties are for 95% confidence intervals.

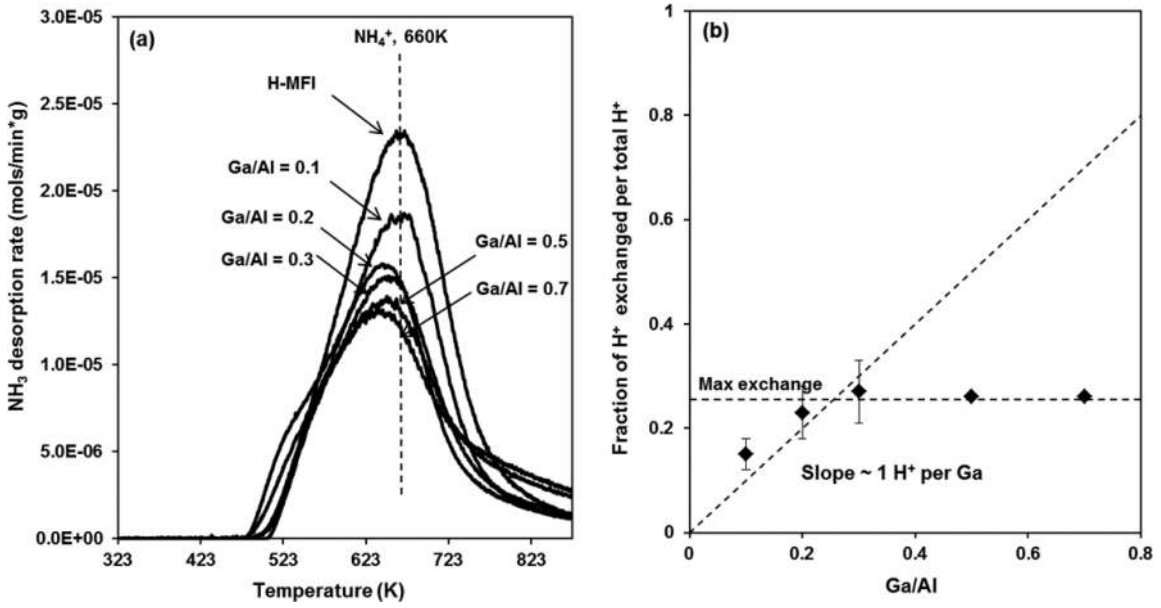

Figure 3. (a) NH_3-TPD profiles (5 K min^{-1}) of H-MFI and Ga-MFI samples with Ga/Al ranging from 0.1 to 0.7. (b) Fraction of H^+ (Brønsted O−H) exchanged per H_{total}^+ determined from NH_3-TPD profiles, as a function of Ga/Al ratio. Dotted lines indicate slope of plot and maximum extent of Brønsted acid O−H exchange. Reported uncertainties are for 95% confidence intervals.

infrared spectra of Ga/H-MFI is most likely attributable to OH groups coordinated to Ga^{3+} centers in either $[Ga(OH)]^{2+}$ or $[Ga(OH)_2]^+$ cations and $[Ga(OH)_2]^+$−H^+ cation pairs.

The fraction of Brønsted acid O−H groups replaced by Ga^{3+} cations can be determined for each Ga/Al ratio on the basis of eq 1 (Experimental and Theoretical Methods) and the integrated area of the ν(O−H) band at 3593 cm^{-1} observed in the infrared spectra of Ga/H-MFI and H-MFI. This fraction is plotted as a function of the Ga/Al ratio in Figure 2b. It is apparent from the slope of this plot (dotted line in Figure 2b) that, for Ga/Al ratios ≤0.3, each Ga^{3+} replaces approximately two Brønsted acid O−H groups. This exchange stoichiometry is consistent with the presence of divalent $[Ga(OH)]^{2+}$ cations that involve the titration of two Brønsted acid O−H groups at proximate cation-exchange sites associated with pairs of framework Al atoms, by one Ga^{3+} atom. Consistent with this interpretation, the fraction of Brønsted acid O−H groups replaced by Ga^{3+} cations reaches a maximum value of approximately 50% at a Ga/Al ratio of ∼0.3. This maximum extent of Brønsted acid O−H exchange is similar to the total fraction of proximate cation-exchange sites associated with pairs of framework Al atoms in our sample of H-MFI (∼45% of Al_f by Co^{2+} titration[27]). This finding suggests that, under oxidizing conditions, Ga^{3+} cations exchange predominantly with Brønsted acid O−H groups at proximate cation-exchange sites, rather than isolated cation-exchange sites. For samples with Ga/Al ratios >0.3, no further exchange of Brønsted acid O−H groups by Ga^{3+} cations is observed in Figure 2a,b. Raman spectroscopy showed no evidence for crystalline β-Ga_2O_3 in any of the Ga/H-MFI samples. Consequently, we hypothesize

DOI: 10.1021/acscatal.8b01254
ACS Catal. 2018, 8, 6106−6126

that an increase in Ga content beyond a Ga/Al ratio of 0.3 leads to the formation of GaO_x oligomers that do not occupy cation-exchange sites. Evidence for the presence of such species will be presented below.

The extent of exchange of Brønsted acid O−H groups by Ga^{3+}cations was also estimated by titrating the residual Brønsted acid O−H groups in Ga/H-MFI with gas-phase NH_3. The protocol used here was that developed by Di Iorio et al. to selectively titrate residual Brønsted acid O−H groups in Cu- and Co-exchanged zeolites, without concomitant titration of Lewis acid sites by NH_3.[60] NH_3-TPD profiles for H-MFI and Ga/H-MFI, shown in Figure 3a, exhibit a single NH_3 desorption feature at 660 K associated with desorption of NH_3 from Brønsted acid O−H groups.[60] This feature decreases in area with increasing Ga content, consistent with the titration of fewer residual Brønsted acid O−H groups in Ga/H-MFI after Ga^{3+} exchange. The NH_3/Al_{tot} value for H-MFI (Table 2) is less than unity: 0.87 ± 0.11, suggesting that approximately 13% of Al_{tot} is not associated with Brønsted acid O−H groups, likely present as EFAl. This estimated Brønsted acid O−H density of 0.87 ± 0.11 H^+/Al_{tot} is also consistent with the value measured using Na^+ exchange protocols (0.84 H^+/Al_{tot}).[27] As observed in Table 2, the value of NH_3/Al_{tot} decreases with increasing Ga content up to Ga/Al ratios of 0.3. For Ga/Al ratios higher than this value, the value of NH_3/Al_{tot} becomes nearly constant, suggesting that exchange of Brønsted acid O−H groups by Ga^{3+} occurs predominantly at proximate cation-exchange sites associated with pairs of framework Al atoms.

Table 2. NH_3/Al_{tot} Ratios for H-MFI and Oxidized Ga/H-MFI Samples, Derived from NH_3-TPD Profiles[a]

sample	NH_3/Al_{tot}[d]
H-MFI[b]	0.87 ± 0.13
Ga/Al[c]	
0.1	0.74 ± 0.13
0.2	0.67 ± 0.09
0.3	0.64 ± 0.11
0.5	0.64
0.7	0.64

[a]Ratios were obtained by integrating the area of the NH_3 desorption feature at 660 K and normalizing the quantity of desorbed NH_3 by the Al_{tot} content. [b]H-MFI, Zeolyst Batch CBV3024E, Si/Al_{tot} = 16.5 ± 1.0 (ICP-OES, Galbraith Laboratories). [c]Elemental compositions determined by ICP-OES (Galbraith Laboratories). [d]Samples were calcined at 773 K for 0.3 h prior to NH_3 saturation at 433 K. After NH_3 saturation, samples at 433 K were purged in 1% H_2O/He for 8 h. Reported uncertainties reflect 95% confidence intervals.

This finding is consistent with the infrared spectroscopy measurements discussed above.

The fraction of Brønsted acid O−H groups exchanged by Ga^{3+} cations at each Ga/Al ratio can be estimated using the measured values of NH_3/Al_{tot} in conjunction with eq 2 (Experimental and Theoretical Methods). The results, plotted as a function of the Ga/Al ratio, are shown in Figure 3b and suggest that, for Ga/Al ratios ≤0.3, each Ga^{3+} center titrates approximately one Brønsted acid O−H group. This exchange stoichiometry is only consistent with Structure 2 in Scheme 1, i.e., $[Ga(OH)_2]^+$−H^+ cation pairs, in contrast to the result obtained from infrared spectroscopy, which suggested that, for Ga/Al ratios ≤0.3, each Ga^{3+} exchanged with two Brønsted acid O−H groups. It should be noted that the exchange stoichiometry of the Ga/Al = 0.1 sample was higher than one Brønsted acid O−H group replaced per Ga^{3+} (1.3 ± 0.3), consistent with the presence of $[Ga(OH)]^{2+}$ cations in addition to $[Ga(OH)_2]^+$−H^+ cation pairs at low Ga/Al ratios. In addition, the maximum extent of exchange of Brønsted acid O−H groups, measured by NH_3-TPD, is approximately 25%. This value is approximately a factor of 2 lower than the maximum extent of Brønsted acid O−H exchange measured via infrared spectroscopy (~50%). The contradiction in exchange stoichiometries estimated by infrared spectroscopy and NH_3-TPD can be resolved by examining the thermodynamics for forming Structures 1 and 2 from their reactants on proximate cation-exchange sites associated with pairs of framework Al atoms.

The Gibbs free energy of formation (ΔG_f) at 773 K and 10^5 Pa for both $[Ga(OH)]^{2+}$ cations (Structure 1) and $[Ga(OH)_2]^+$−H^+ cation pairs (Structure 2) was estimated starting from $GaCl_3$, H_2, O_2, and two proximate Brønsted acid O−H groups associated with NNN and NNNN pairs of framework Al atoms. Given the distribution of framework Al atoms among different crystallographic positions in the zeolite framework, the Al−Al interatomic distance between proximate cation-exchange sites is likely to vary considerably. While current experimental and theoretical methods do not allow estimation of the distribution of Al site pairs in terms of interatomic framework Al−Al distances in our zeolite samples, the two types of proximate cation-exchange sites used here provide benchmarks for two representative classes of Al−Al site pairs. For optimized structures involving NNN pairs of Al framework atoms, the interatomic Al−Al distances are ≤5 Å, while for optimized structures involving NNNN pairs of framework Al atoms, the interatomic Al−Al distances are >5 Å. The formation of isolated $[Ga(OH)_2]^+$ cations from the same set of reactants and a Brønsted-acid O−H group associated with an isolated framework Al atom in the T12 position was also considered.

Table 3. QM/MM Derived Gibbs Free Energies of Formation of $[Ga(OH)]^{2+}$ Cations and $[Ga(OH)_2]^+$ Cations and $[Ga(OH)_2]^+$−H^+ Cation Pairs from $GaCl_3$, H_2, O_2, and H^+ (Brønsted Acid O−H Groups) at Isolated Cation-Exchange Sites (Denoted as H^+Z^-) and Proximate Cation-Exchange Sites (NNN and NNNN Pairs of Framework Al Atoms; Denoted as $2H^+Z^-$ and Shown in Figure 1) at 773 K (10^5 Pa Pressure)

reactions	Al site type	ΔG_f (at 773 K)[a] (kJ/mol)
$GaCl_3 + 2H_2 + O_2 + H^+Z^- \rightarrow [Ga(OH)_2]^+Z^- + 3HCl$	isolated	−338
$GaCl_3 + 2H_2 + O_2 + 2H^+Z^- \rightarrow [Ga(OH)]^{2+}2Z^- + 3HCl + H_2O$	NNN	−352
	NNNN	−296
$GaCl_3 + 2H_2 + O_2 + 2H^+Z^- \rightarrow [Ga(OH)_2]^+$−$H^+$ $2Z^- + 3HCl$	NNN	−379
	NNNN	−384

[a]Energies calculated at 10^5 Pa total pressure.

DOI: 10.1021/acscatal.8b01254
ACS Catal. 2018, 8, 6106−6126

The Gibbs free energies of formation (ΔG_f) obtained for $[Ga(OH)]^{2+}$ cations, $[Ga(OH)_2]^+$−H^+ cation pairs, and isolated $[Ga(OH)_2]^+$ cations are shown in Table 3. It is apparent that the formation of $[Ga(OH)_2]^+$−H^+ cation pairs at proximate cation-exchange sites associated with pairs of framework Al atoms is more favorable (ΔG_f = −379 kJ/mol and ΔG_f = −384 kJ/mol on NNN and NNNN pairs of framework Al, respectively) than the formation of $[Ga(OH)_2]^+$ cations at cation-exchange sites associated with isolated framework Al atoms (ΔG_f = −338 kJ/mol). In addition to electrostatic stabilization by the anionic zeolite framework, the $[Ga(OH)_2]^+$ cation in a $[Ga(OH)_2]^+$−H^+ cation pair is additionally stabilized via H-bonding between the Ga-bound OH group and the proximate Brønsted acid O−H group. The data in Table 3 also suggest that the formation of $[Ga(OH)_2]^+$−H^+ cation pairs at proximate cation-exchange sites associated with NNNN pairs of framework Al atoms is significantly more favorable than the formation of divalent $[Ga(OH)]^{2+}$ cations at such cation-exchange sites (ΔG_f = −296 kJ/mol). The Ga^{3+} center in a divalent $[Ga(OH)]^{2+}$ cation is under considerable conformational strain resulting from the need to form a tetrahedron with 3 framework O atoms and 1 OH group. This conformational strain likely destabilizes the $[Ga(OH)]^{2+}$ structure relative to the $[Ga(OH)_2]^+$−H^+ cation pair structure, for which the Ga^{3+} center can form a less strained tetrahedron with 2 framework O atoms and 2 OH groups. As noted above, H-bonding between the Ga-bound OH group and the proximate Brønsted acid O−H group may further stabilize this structure. On the other hand, at proximate cation-exchange sites associated with NNN pairs of framework Al atoms, the formation of $[Ga(OH)]^{2+}$ cations is only slightly less favorable (ΔG_f = −352 kJ/mol) than the formation of $[Ga(OH)_2]^+$−H^+ cation pairs (ΔG_f = −379 kJ/mol). This suggests that, at lower H_2O partial pressures (≤10 Pa H_2O for dehydrated zeolites), $[Ga(OH)]^{2+}$ cations will be increasingly thermodynamically favored over $[Ga(OH)_2]^+$−H^+ cation pairs at proximate cation-exchange sites with shorter Al−Al interatomic distances, such as those associated with NNN pairs of framework Al atoms (also see thermodynamic phase diagrams presented in Section 3.3). These findings highlight the sensitivity of Ga^{3+} structures to the interatomic distance between Al atoms in proximate cation-exchange sites: shorter interatomic Al−Al distances allow the Ga^{3+} center to bridge both cation-exchange sites with a lower conformational strain to form divalent $[Ga(OH)]^{2+}$ cations, while longer interatomic Al−Al distances inhibit the formation of such structures, resulting instead in the formation of $[Ga(OH)_2]^+$−H^+ cation pairs.

Our theoretical calculations also suggest that, for $[Ga(OH)_2]^+$−H^+ cation pairs, H-bonding between the Ga-bound OH group and the proximate Brønsted acid O−H group shifts the O−H stretching frequency of the proximate Brønsted acid O−H group to 2436 cm^{-1}, a value significantly lower than that for an isolated Brønsted acid O−H group, 3610 cm^{-1}. This suggests that the proximate Brønsted acid O−H group in $[Ga(OH)_2]^+$−H^+ pairs would be masked by the strong infrared absorption of the zeolite framework. The presence of a single infrared band reflecting this Brønsted acid O−H group is also unlikely, since the red-shift in the O−H stretching frequency may also depend on the proximity between Ga-bound OH groups and their corresponding proximate Brønsted acid O−H groups. This proximity is in turn expected to depend on the interatomic Al−Al distance in proximate cation-exchange sites. Therefore, the presence of either $[Ga(OH)]^{2+}$ cations or $[Ga(OH)_2]^+$−H^+ cation pairs would result in an apparent exchange stoichiometry of two Brønsted acid O−H groups replaced per Ga^{3+} atom as measured via infrared spectroscopy monitored at 3593 cm^{-1}. The proximate Brønsted acid O−H group in $[Ga(OH)_2]^+$−H^+ cation pairs should, in principle, be detectable by titration with NH_3. This structure should therefore result in an exchange stoichiometry of one Brønsted acid O−H group replaced per Ga^{3+} atom, as measured via NH_3-TPD. Furthermore, for low Ga/Al ratios (∼0.1), NH_3-TPD indicates that between one and two Brønsted O−H groups are replaced per Ga^{3+} atom, suggesting that $[Ga(OH)]^{2+}$ cations may also form in addition to $[Ga(OH)_2]^+$−H^+ cation pairs at low Ga/Al ratios. If Ga^{3+} siting is assumed to be thermodynamically controlled, it is plausible that, at low Ga/Al ratios, the most stable $[Ga(OH)_2]^+$−H^+ cation pairs form at proximate cation-exchange sites associated with pairs of framework Al atoms with Al−Al interatomic distances ≤5 Å. For low H_2O partial pressures (≤10 Pa), such structures may readily undergo condensation to form $[Ga(OH)]^{2+}$ cations, a conclusion supported by the phase diagrams presented in Figure 9. We therefore conclude on the basis of infrared spectroscopy, NH_3-TPD, and theoretical calculations that, for Ga/Al ratios ∼0.1, $[Ga(OH)]^{2+}$ cations form at proximate cation-exchange sites associated with pairs of framework Al atoms with Al−Al interatomic distances ≤5 Å. On the other hand, $[Ga(OH)_2]^+$−H^+ cation pairs form in greater proportion at proximate cation-exchange sites associated with pairs of framework Al atoms for which the Al−Al distances are >5 Å for Ga/Al ratios between 0.1 and 0.3. The concentration of $[Ga(OH)_2]^+$−H^+ cation pairs increases with increasing Ga/Al ratio until all proximate cation-exchange sites associated with pairs of framework Al atoms are saturated. For Ga/Al ratios higher than ∼0.3, the formation of neutral GaO_x species occurs. Such species may be formed via hydrolysis of $[Ga(OH)_2]^+$ cations associated with isolated cation-exchange sites during the oxidation of the H_2-reduced Ga/H-MFI at 773 K in O_2.

Further evidence supporting the formation of $[Ga(OH)_2]^+$−H^+ cation pairs was obtained from Ga K-edge X-ray absorption spectroscopy (XAS). XANES spectra of Ga/H-MFI and of two Ga^{3+} standards, β-Ga_2O_3 and $Ga(acac)_3$, are shown in Figure 4. The Ga K-edge energy, defined as the lowest energy inflection in the first derivative of the absorption edge region of the XAS spectrum, was measured for both Ga^{3+} standards and Ga/H-MFI samples (at 773 K under O_2); these values are shown in Table 4. The Ga K-edge energies for Ga/H-MFI samples (∼10 374.0−10 375.1 eV) are similar to those of the Ga^{3+} standards (10 375.1 eV for β-Ga_2O_3 and 10 376.6 eV for $Ga(acac)_3$), confirming that Ga^{3+} cations in Ga/H-MFI samples have an oxidation state of +3 and are coordinated to O atoms. The maximum of the absorption intensity in the edge region for all Ga/H-MFI samples occurs at approximately 10 376 eV (Figure 4). The XANES spectra of β-Ga_2O_3 (Figure 4) shows two maxima in the edge region, one at 10 376 eV and the other at 10 379 eV, whereas the XANES spectrum of $Ga(acac)_3$ shows a single maximum in the edge region at 10 379 eV. The XANES spectra of aqueous Ga−O complexes exhibit absorption intensity maxima at 10 378 eV for tetrahedral Ga−O complexes and at 10379 eV for octahedral Ga−O complexes.[61] These findings are consistent with the observation of two maxima in the XANES spectrum of β-Ga_2O_3, which contains Ga^{3+} in both tetrahedral and octahedral coordination with O atoms,[62] and the observation of only the higher energy

DOI: 10.1021/acscatal.8b01254
ACS Catal. 2018, 8, 6106−6126

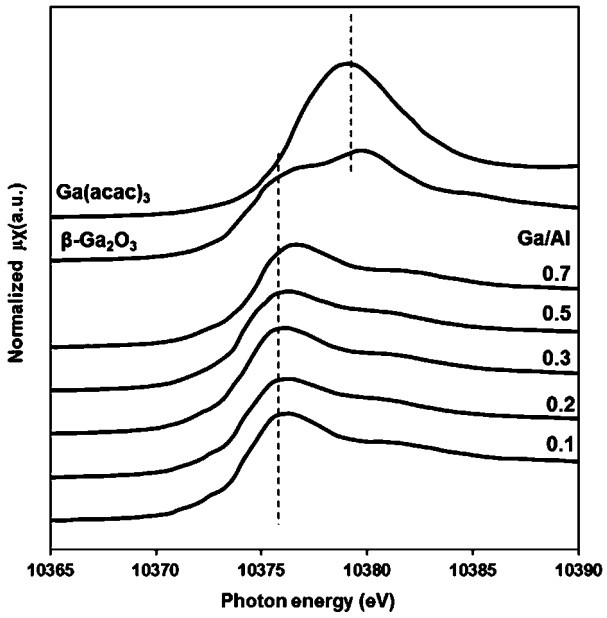

Figure 4. Normalized Ga K-edge X-ray absorption near edge spectra (XANES) for Ga/H-MFI samples, collected at 773 K under flowing 20% O_2/He. Also shown are XANES spectra for β-Ga_2O_3 and $Ga(acac)_3$, collected at ambient temperatures. Dotted lines indicate positions of absorption maxima.

Table 4. Ga K-Edge XANES Edge Energies of Ga^{3+} Standards (at Ambient Conditions) and Ga/H-MFI Samples, Measured at 773 K under Flowing 20% O_2/He

sample	XANES edge energy (eV)[a]
β-Ga_2O_3[b]	10375.1
$Ga(acac)_3$[b]	10376.6
Ga/Al (measured)[c]	
0.1	10374.3
0.2	10374.0
0.3	10375.0
0.5	10375.1
0.7	10375.0

[a]Edge energies are defined as the lowest energy inflection point in the edge region of the first derivative of the XANES spectrum. [b]Powdered standards (acquired from Sigma-Aldrich and Strem Chemical) were spread on Kapton tape, which was then folded to yield an approximate absorption length of 2. [c]Ga/H-MFI samples (~0.01 g) were pressed into self-supporting pellets and installed in a six-shooter sample holder inside the in situ XAS cell.

maximum (~10 379 eV) in $Ga(acac)_3$, which contains Ga^{3+} only in octahedral coordination with O atoms.[63] Therefore, the observation in Figure 4 of a single absorption maximum at 10 376 eV for XANES spectra of all Ga/H-MFI suggests that exchanged Ga^{3+} cations are tetrahedrally coordinated with O atoms at all Ga/Al ratios.

EXAFS spectra (k^2-weighted) of Ga/H-MFI samples (shown in Figure S.8) were Fourier-transformed (FT) and analyzed in order to determine the structure of Ga^{3+} cations around the first coordination shell. The magnitudes of the (k^2-weighted) FT Ga K-edge EXAFS spectra of Ga/H-MFI samples, collected at 773 K under flowing 20% O_2/He, are shown in Figure 5. For Ga/H-MFI samples with Ga/Al ratios <0.2, sufficient X-ray absorption could not be achieved due to the low Ga content of these samples (<1 wt % Ga). As a result, our EXAFS analysis is

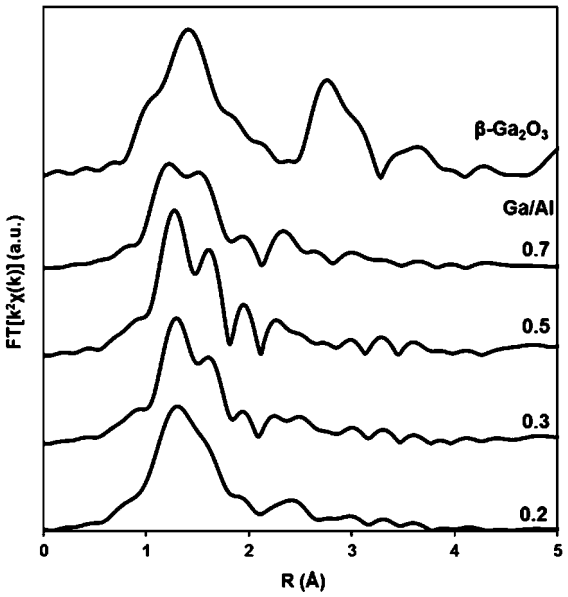

Figure 5. Magnitudes of k^2-weighted Fourier-transformed Ga K-edge EXAFS spectra of β-Ga_2O_3 measured at ambient temperature and of Ga/H-MFI samples (Ga/Al = 0.2–0.7) measured at 773 K under 20% O_2/He.

limited to Ga/H-MFI with Ga/Al ratios ≥0.2. Also shown in Figure 5 is the magnitude of the FT-EXAFS spectrum of β-Ga_2O_3. The peak positions in these spectra do not correspond to exact interatomic distances, due to the phase shifts incurred by photoelectrons from absorbing and scattering atoms and, therefore, peak maxima appear 0.3–0.5 Å lower than true interatomic distances.[64] Fourier-transformed EXAFS spectra of all Ga/H-MFI samples and β-Ga_2O_3 (Figure 5) show dominant features between 1 and 2 Å in R-space corresponding to backscattering from O atoms coordinated to Ga^{3+} centers. The FT spectra of β-Ga_2O_3 in Figure 5 exhibits a large peak between 2 and 3 Å, corresponding to backscattering from next-neighbor Ga atoms in Ga–O–Ga linkages. The second coordination shell in the EXAFS spectra of all Ga/H-MFI samples also show features between 2 and 3 Å that are less intense than the feature in the EXAFS of β-Ga_2O_3. These features correspond to backscattering from framework Al or Si or extra-framework Ga atoms (for example, in condensed GaO_x species).

EXAFS fitting of the first coordination shell was undertaken for spectra of Ga/H-MFI samples in order to determine the average number of neighboring O atoms and their interatomic distances from Ga^{3+} centers. The procedure used for EXAFS fits is outlined in detail in the Text S.5.

Satisfactory fits of the spectra were obtained for all Ga/H-MFI samples, as evidenced by the close agreement between dotted lines and the solid lines shown in Figure S.9a–d for the first-coordination shell. Fitted parameters for Ga/H-MFI spectra are presented in Table 5. These results suggest that, on average, each Ga^{3+} center is coordinated to 2 O atoms at an interatomic distance of approximately 1.77 Å and to 2 O atoms at an interatomic distance of approximately 1.92 Å. This interatomic bonding is consistent with the structure of tetrahedral $[Ga(OH)_2]^+$ cations, for which theoretical simulations (see Figures S.5–S.7 for theoretically generated structures) indicate that the Ga^{3+} cation is coordinated to 2 OH groups with a Ga–O interatomic distance of 1.79 Å and to 2 framework O atoms at a Ga–O interatomic distance of 1.99

DOI: 10.1021/acscatal.8b01254
ACS Catal. 2018, 8, 6106–6126

Table 5. Fitted Coordination Numbers, Interatomic Distances, Debye-Waller Factors, Energy Shift Parameters, and R-Factor Values for Fits to Fourier-Transformed Ga K-Edge EXAFS of Ga/H-MFI Samples at 773 K under Flowing 20% O_2/He[a]

Ga/Al[b]	Ga−O shell[c]	N_i[d]	total N	R_i[e] (Å)	σ^2[f] (10^{-3} Å^2)	ΔE_0[g] (eV)	R-factor (10^{-2})
0.2	Ga−O_1	2.0	3.9	1.77	4.0	3.1	0.7
	Ga−O_2	1.9		1.92			
0.3	Ga−O_1	1.7	3.5	1.77	1.0	2.6	2.2
	Ga−O_2	1.8		1.93			
0.5	Ga−O_1	1.7	3.8	1.75	0.1	1.7	2.1
	Ga−O_2	2.1		1.92			
0.7	Ga−O_1	1.5	3.8	1.73	3.2	1.3	1.4
	Ga−O_2	2.3		1.90			

[a]Fits were performed using $CaGa_2O_4$ as a model structure. [b]Samples were pressed into self-supporting pellets into the sample holder in an in situ cell. Measurements were conducted at 773 K under flowing 20% O_2/He. EXAFS spectra, obtained after normalization and background subtraction, were k^2-weighted; a Hanning window function was applied between k = 2−14 Å^{-1}, and first shell fits were performed from R = 1−2.1 Å. S_0^2 values were determined to be 0.94, by fitting experimental EXAFS spectra of β-Ga_2O_3 to Ga−O shells generated using the crystal structure of β-Ga_2O_3[69] in FEFF. [c]Two Ga−O shells were generated in FEFF using the crystal structure of $CaGa_2O_4$ which was obtained from ref 33. [d]Coordination numbers (N_i where i = 1−2) for each shell were determined with a ±0.60 uncertainty. [e]Ga−O interatomic distances (R_i where i = 1−2) for each shell were determined with a ±0.04 Å uncertainty. [f]Debye−Waller factors (σ^2) were held the same for each shell. [g]Energy shift parameters (E_0) were determined with a ±2 eV uncertainty.

Å. The fitted interatomic distance assigned to bonding between Ga^{3+} and Ga-bound OH groups (~1.77 Å) agrees well with measured values for aqueous tetrahedral $Ga(OH)_4^-$ complexes for which the Ga−O interatomic distance is ~1.80 Å.[61] The fitted interatomic distance between Ga^{3+} and framework O atoms (~1.92 Å) is approximately 0.07 Å lower than the distance for these bonds determined from our DFT calculations (~1.99 Å). It should be noted that exact agreement between theoretical predictions of interatomic distances and values obtained from EXAFS fits is not expected. This discrepancy is well-documented and is ascribed to the effects of structural and thermal disorder on the absorber−scatterer interatomic pair distribution, which is assumed to have a Gaussian form in the conventional EXAFS equation.[65−67] A high degree of thermal and structural disorder (typical for measurements on highly dispersed metal sites in solids at high temperatures) may skew this pair distribution, leading to slightly lower fitted interatomic distances when conventional EXAFS analysis is used.[68]

From the preceding discussion, it is clear that, under oxidizing conditions, exchange of Brønsted acid O−H groups by Ga^{3+} results in a saturation of proximate cation-exchange sites associated with pairs (NNN or NNNN) of framework Al atoms at a Ga/Al ratio of ~0.3. EXAFS analysis of the first coordination shell around Ga^{3+} centers (Table 5), however, suggests that exchanged Ga^{3+} cations and neutral GaO_x species (present at Ga/Al ratios >0.3) are both predominantly tetrahedrally ligated to O atoms. In the second-coordination shell, however, isolated Ga^{3+} cations are expected to be proximate to framework Al or Si atoms only. On the other hand, Ga^{3+} centers in multinuclear cationic Ga^{3+} species such as the $[Ga_2O_2]^{2+}$ structures proposed by Hensen et al.,[17] or in neutral GaO_x species, are expected to be proximate to extra-framework Ga^{3+} atoms, via Ga−O−Ga linkages. Evidence for $[Ga(OH)_2]^+$−H^+ cation pairs at Ga/Al ratios ≤0.3 and for the formation of GaO_x species at Ga/Al ratios >0.3 was obtained by wavelet analyses of the EXAFS spectra. This method of EXAFS data analysis allows the construction of a two-dimensional picture that enables the wavenumber space (k-space) and radial space (R-space) dependence of the EXAFS signal to be examined simultaneously.[34,70−74] A maximum in the wavelet transform occurs when the frequency and amplitude components in the transformed signal coincide with those in the wavelet.[34] A detailed description of the methods used to compute wavelet transforms of simulated Ga^{3+} structures and of experimentally measured EXAFS data is included in the Text S.6.

The wavelet transform of the k^2-weighted EXAFS spectrum of the simulated $[Ga(OH)_2]^+$ cation (Figure 6a) shows a single intense feature in the second coordination shell at R = 2.5 Å in R-space and between 3 and 8 Å^{-1} in k-space, due to backscattering from the framework Al atom associated with the cation-exchange site. On the other hand, the wavelet transform of the experimentally measured EXAFS spectrum of β-Ga_2O_3 (Figure 6b) shows a single intense feature in the

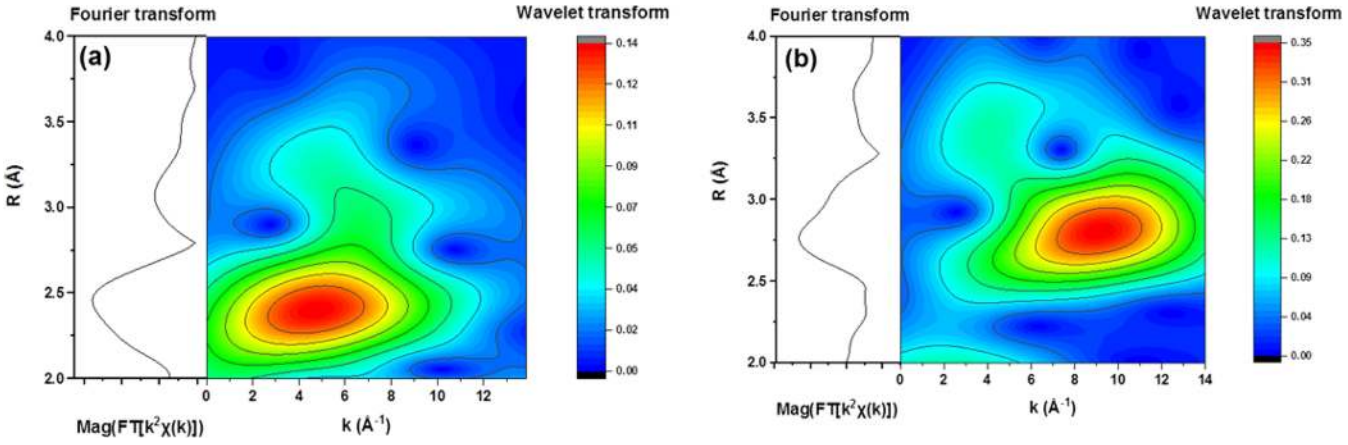

Figure 6. Wavelet transforms of the second coordination shell (2< R < 4 Å) of k^2-weighted Ga K-edge EXAFS spectra for (a) DFT-simulated isolated $[Ga(OH)_2]^+$ cation and (b) β-Ga_2O_3 measured at ambient temperature. Wavelet transforms were computed in the HAMA software[34] using a Morlet wavelet function with $\kappa\sigma$ values set to 15. See Text S.6 for details on the methods used to compute Figure 7.

DOI: 10.1021/acscatal.8b01254
ACS Catal. 2018, 8, 6106−6126

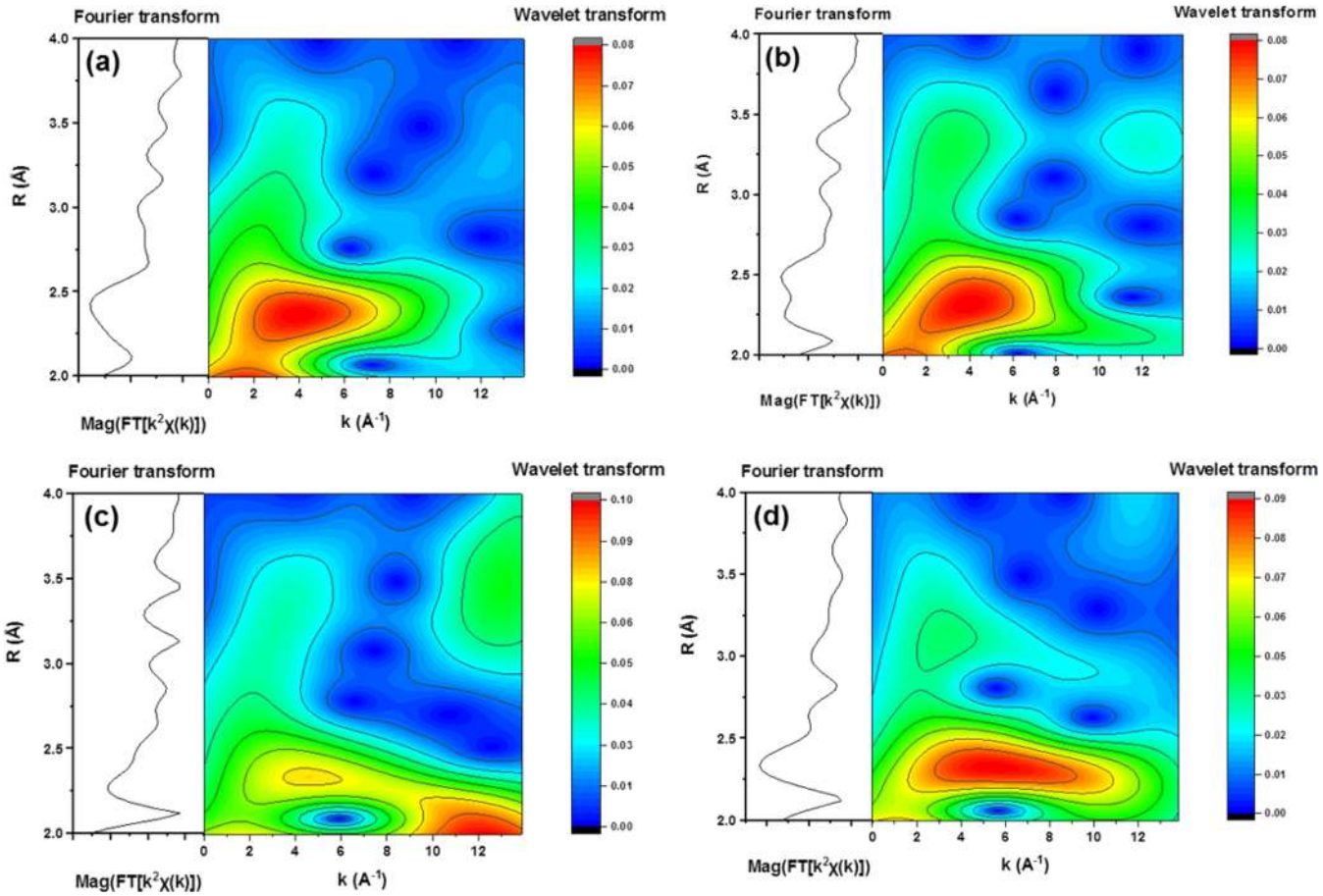

Figure 7. Wavelet transforms of the second coordination shell of k^2-weighted Ga K-edge EXAFS spectra of Ga/H-MFI samples, measured at 773 K under flowing 20% O_2/He: (a) Ga/Al = 0.2, (b) Ga/Al = 0.3, (c) Ga/Al = 0.5, and (d) Ga/Al = 0.7. Wavelet transforms were computed using the HAMA software[34] using a Morlet wavelet function with $\kappa\sigma$ values set to 15. See Text S.6 for details on the methods used to compute Figure 7.

second coordination shell at R = 2.7 Å in R-space and between 7 and 13 $Å^{-1}$ in k-space, due to backscattering from next-nearest neighboring Ga atoms. It is apparent that, while framework Al atoms associated with $[Ga(OH)_2]^+$ cations and next-nearest neighboring Ga atoms in β-Ga_2O_3 are at similar interatomic distances from Ga^{3+} centers, they exhibit very different k-space dependences. It has been shown that, in general, atoms with higher atomic numbers exhibit maxima in their backscattering amplitudes at higher wavenumbers (values of k) than atoms with lower atomic numbers.[64] Ga atoms, with their higher atomic number (Z = 31) exhibit a wavelet maximum at higher k values than that observed for the wavelet maximum of Al atoms (Z = 13). The wavelet transforms of k^2-weighted EXAFS spectra of Ga/H-MFI with Ga/Al ratios ≤0.3 (i.e., Ga/Al = 0.2, 0.3; Figure 7a,b) show a single dominant feature in the second coordination shell at 2.5 Å in R-space and 3−8 $Å^{-1}$ in k-space, consistent with backscattering from framework Al atoms. This finding confirms that Ga^{3+} cations in samples with Ga/Al ≤ 0.3 do not possess other extra-framework Ga^{3+} atoms in their vicinity and are therefore site isolated. Wavelet transforms of k^2-weighted EXAFS spectra of Ga/H-MFI with Ga/Al ratios >0.3 (i.e., Ga/Al = 0.5, 0.7; Figure 7c,d) also show the feature associated with Al backscattering in the second coordination shell. However, a second, overlapping feature is also observed in these spectra with wavelet coordinates (R = 2.2−3.0 Å and k = 7−13 $Å^{-1}$) consistent with backscattering from Ga atoms. This finding suggests that, at Ga contents higher than Ga/Al ∼ 0.3, Ga^{3+} species containing condensed Ga−O−Ga linkages coexist with exchanged $[Ga(OH)]^{2+}$ cations and $[Ga(OH)_2]^+$−H^+ cation pairs.

The data presented and discussed above suggest that, for Ga/Al ratios ≤0.3, isolated $[Ga(OH)]^{2+}$ cations and $[Ga(OH)_2]^+$−H^+ pairs form at proximate cation-exchange sites associated with pairs of framework Al atoms. The population of the latter structure increases with increasing Ga loading, until the available proximate cation-exchange sites are saturated at a Ga/Al ratio of ∼0.3. The addition of Ga in excess of this saturation stoichiometry leads to Ga^{3+} structures in oxidized Ga/H-MFI with condensed Ga−O−Ga linkages that do not appear to be ion-exchanged at cation-exchange sites. Our data are therefore not consistent with the presence of binuclear $[Ga_2O_2]^{2+}$ cations at Ga/Al ratios >0.3, as proposed by Hensen et al.[17] We suggest instead that the addition of Ga at levels higher than Ga/Al ratios of 0.3 leads to the formation of weakly bound $[Ga(OH)_2]^+$ cations at residual cation-exchange sites associated with isolated framework Al atoms. In the presence of trace levels of H_2O during calcination, these structures may de-anchor via reaction of $[Ga(OH)_2]^+$ with H_2O to form a Brønsted acid O−H group and mobile $Ga(OH)_3$ species, which may undergo subsequent condensation to form neutral, GaO_x oligomers with structures that may resemble the Ga_4O_4 complexes proposed by Faro et al.[75] As noted above, Ga−O−Ga linkages in these structures are detectable by wavelet

DOI: 10.1021/acscatal.8b01254
ACS Catal. 2018, 8, 6106−6126

Scheme 2. Pathways for Reactions of $[Ga(OH)]^{2+}$ Cations and $[Ga(OH)_2]^{+}-H^{+}$ Cation Pairs, with H_2 To Generate Structure 3, $[Ga(OH)H]^{+}-H^{+}$ Cation Pairs, Structure 4, $[GaH]^{2+}$ Cations, and Structure 5, $[GaH_2]^{+}-H^{+}$ Cation Pairs

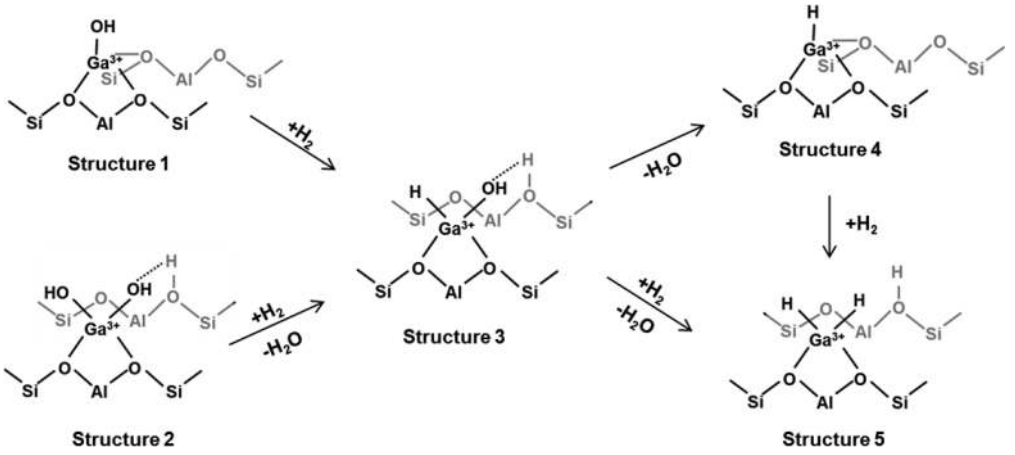

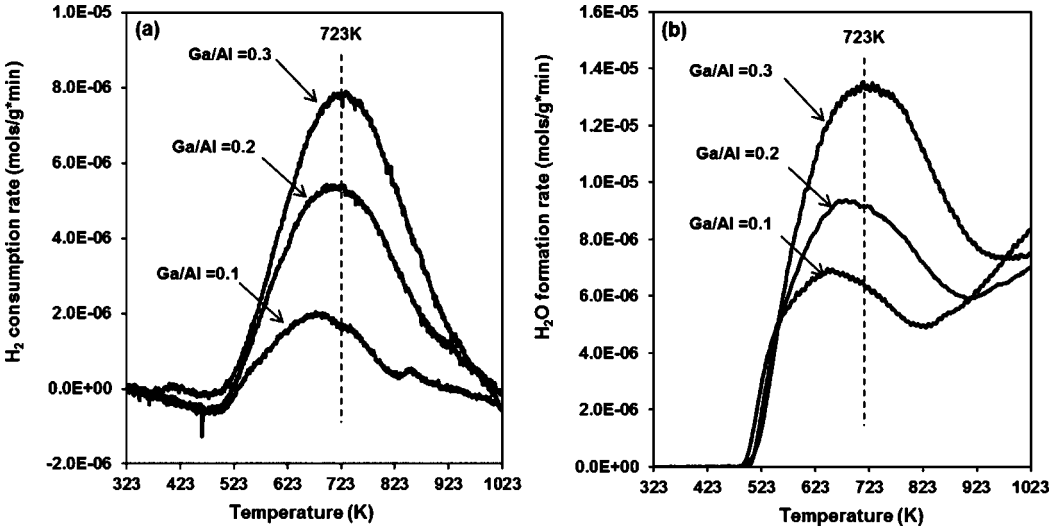

Figure 8. H_2-temperature programmed reduction (H_2-TPR) profiles (10 K min^{-1}) for Ga/H-MFI samples (Ga/Al = 0.1−0.3). (a) H_2 consumption rates per g. (b) H_2O formation rates per g. Integrated H_2/Ga and H_2O/Ga ratios are tabulated in Table 6.

analysis of the EXAFS spectra. Our data, however, do not let us discern whether the GaO_x species are located inside the zeolite micropores or on the surface of the zeolite crystals.

3.3. The State of Ga^{3+} Cations in H_2-Treated Ga/H-MFI.

We next report our findings on the structure of Ga^{3+} species produced by H_2 reduction of oxidized Ga/H-MFI. Scheme 2 illustrates several pathways by which $[Ga(OH)]^{2+}$ cations and $[Ga(OH)_2]^{+}-H^{+}$ cation pairs at proximate cation-exchange sites associated with pairs of framework Al atoms might undergo reduction. According to this scheme, the reaction between divalent $[Ga(OH)]^{2+}$ cations (Structure 1) and one equivalent of H_2 could result in the reprotonation of one cation-exchange site and the formation of $[Ga(OH)H]^{+}-H^{+}$ cation pairs (Structure 3). $[Ga(OH)_2]^{+}-H^{+}$ cation pairs (Structure 2) may also react with one equivalent of H_2 to form $[Ga(OH)H]^{+}-H^{+}$ cation pairs (Structure 3) and 1 equiv of H_2O. $[Ga(OH)H]^{+}$ cations may undergo condensation with the proximate Brønsted acid O−H group to form $[GaH]^{2+}$ cations (Structure 4) and form one equivalent of H_2O. Alternatively, $[Ga(OH)H]^{+}-H^{+}$ cation pairs could further react with one equivalent of H_2 to form $[GaH_2]^{+}-H^{+}$ cation pairs (Structure 5) and one equivalent of H_2O.

H_2-temperature programmed reduction (H_2-TPR) profiles of Ga/H-MFI with Ga/Al ratios of 0.1−0.3 are shown in Figure 8, as the molar consumption rate of H_2 per gram of catalyst (Figure 8a) and as the molar formation rate of H_2O per gram of catalyst (Figure 8b). A single H_2 consumption and H_2O formation peak is observed at 723 K for all three Ga/H-MFI samples; the intensities of these features increase with increasing Ga content. The H_2O formation profiles for Ga/H-MFI (Figure 8b) exhibit an additional feature for H_2O formation at temperatures >823 K. This feature was also observed in the H_2-TPR profile of H-MFI and is likely due to dehydroxylation of proximate Si−OH groups and of framework Al atoms that undergo dealumination at temperatures >1000 K.[76,77]

The area under the H_2 consumption and H_2O generation peaks can be integrated to assess the molar consumption of H_2 and the molar formation of H_2O per Ga atom. Integrated H_2O molar yields for Ga/H-MFI samples were corrected for H_2O desorption from the zeolite by subtracting the integrated H_2O molar yield for H-MFI from that of Ga/H-MFI. These data, presented in Table 6, suggest that, for Ga/Al ratios of 0.1 to 0.3, approximately 1 equivalent of H_2 is consumed per Ga atom.

DOI: 10.1021/acscatal.8b01254
ACS Catal. 2018, 8, 6106−6126

Table 6. Integrated H_2/Ga, H_2O/Ga, and H_2O/H_2 Ratios for H_2-TPR Profiles of Ga/H-MFI Samples (Ga/Al = 0.1 to 0.3) and H^+_{exch}/H^+_{total} and H^+_{exch}/Ga Values Measured via NH_3-TPD after H_2 Treatment of Ga/H-MFI Samples at 823 K

Ga/Al	H_2/Ga[a]	H_2O/Ga[a]	H_2O/H_2	H^+_{exch}/H^+_{tot}	H^+_{exch}/Ga[b]
0.1	0.8	1.3	1.7	0.25	2.2
0.2	0.8	1.1	1.3	0.34	1.5
0.3	0.8	1.1	1.4	0.41	1.2

[a]Ratios were obtained by integrating the area of H_2 molar consumption and the H_2O molar formation feature at 723 K and normalizing these areas by the molar Ga content. Integrated H_2O formation was corrected for H_2O desorption from H-MFI using the H_2-TPR profile of H-MFI. [b]Obtained from NH_3-TPD profiles of H_2-treated Ga/H-MFI samples. NH_3/Al_{tot} values from these experiments were used together with eq 2 in order to estimate H^+_{exch}/H^+_{tot}. These values were then normalized by the Ga/Al_f ratio (obtained by dividing Ga/Al_{tot} values by the Al_f/Al_{tot} value for H-MFI) in order to obtain values of H^+_{exch}/Ga.

For Ga/Al ratios ≤0.1, these data are consistent with the reduction of $[Ga(OH)]^{2+}$ cations (~30% of the Ga^{3+} in oxidized Ga/Al = 0.1 sample, by NH_3-TPD) to either $[Ga(OH)H]^+-H^+$ cation pairs or divalent $[GaH]^{2+}$ cations. H_2/Ga ratios of 1 are also consistent with the reduction of $[Ga(OH)_2]^+-H^+$ cation pairs to either $[Ga(OH)H]^+-H^+$ cation pairs (Structure 3) or divalent $[GaH]^{2+}$ cations (Structure 4). However, the observed H_2 consumption ratios are not consistent with the reduction of $[Ga(OH)]^{2+}$ or $[Ga(OH)_2]^+-H^+$ cation pairs to $[GaH_2]^+-H^+$ cation pairs (Structure 5), since both reactions require the consumption of two equivalents of H_2 per Ga atom. The formation of $[Ga(OH)H]^+-H^+$ cation pairs and $[GaH]^{2+}$ cations from $[Ga(OH)]^{2+}$ cations requires the formation of zero and one equivalents of H_2O, respectively, while the formation of these two structures from $[Ga(OH)_2]^+-H^+$ cation pairs would require the formation of one and two equivalents of H_2O, respectively. Measured H_2O/Ga and H_2O/H_2 ratios determined from H_2-TPR profiles for all three Ga/H-MFI samples (Table 6) are greater than 1 but less than 2, with values decreasing closer to unity with increasing Ga/Al ratio. These data suggest that, under the conditions prevailing during H_2-TPR, $[Ga(OH)]^{2+}$ cations and $[Ga(OH)_2]^+-H^+$ cation pairs convert to both $[GaH]^{2+}$ cations and $[Ga(OH)H]^+-H^+$ cation pairs; $[GaH]^{2+}$ cations appear to be present at all Ga/Al ratios but in a higher proportion at lower Ga/Al ratios.

Also shown in Table 6 is the fraction of Brønsted acid O−H groups replaced by Ga^{3+} for H_2-treated Ga/H-MFI samples, determined from NH_3-TPD. Exchange stoichiometries determined from these data suggest that, for the Ga/Al = 0.1 sample, two Brønsted acid O−H groups are replaced per Ga^{3+} atom, consistent with the presence of $[GaH]^{2+}$ cations in this sample after H_2 treatment. With an increase in Ga content (up to a Ga/Al ratio of 0.3), the exchange stoichiometry of H_2-treated Ga/H-MFI decreases to between one and two Brønsted acid O−H groups replaced per Ga^{3+} atom, consistent with a higher concentration of $[Ga(OH)H]^+-H^+$ cation pairs as the Ga/Al ratio increases. In conclusion, NH_3-TPD and H_2-TPR data provide evidence for the formation of $[GaH]^{2+}$ cations at low Ga/Al ratios (Ga/Al = 0.1) and the formation of $[Ga(OH)H]^+-H^+$ cation pairs in increasing concentration for Ga/Al ratios between 0.1 and 0.3.

We have shown above that, under oxidizing conditions, the formation of $[Ga(OH)]^{2+}$ cations at proximate cation-exchange sites depends sensitively on the framework Al−Al interatomic distance and H_2O partial pressure. In an analogous manner, we propose that the stability of $[GaH]^{2+}$ cations and their tendency to decompose into $[Ga(OH)H]^+-H^+$ or $[GaH_2]^+-H^+$ cation pairs depends on both the framework Al−Al interatomic distance between proximate cation-exchange sites and the partial pressures of H_2 and H_2O. To assess the validity of this hypothesis, we generated theoretical phase diagrams in order to illustrate the regions of stability for various Ga^{3+} structures as a function of temperature and H_2 partial pressure for a given H_2O partial pressure. Each region of stability in these phase diagrams is representative of a Ga^{3+} structure that exhibits the lowest free energy of formation from $[Ga(OH)_2]^+-H^+$ cation pairs. Equations 3 and 4 (Experimental and Theoretical Methods) were used to calculate these free energies of

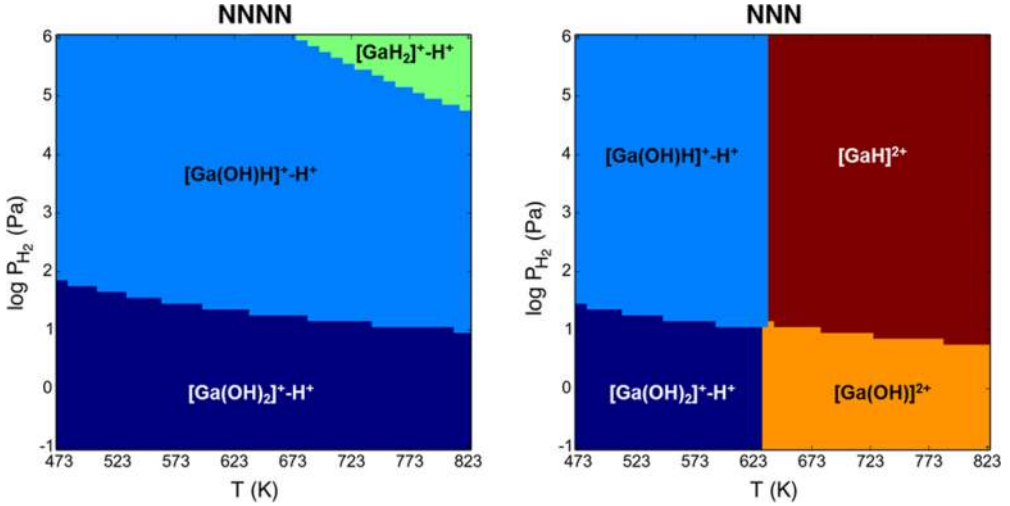

Figure 9. Theoretical thermodynamic phase diagrams for Ga^{3+} structures at cation-exchange sites associated with NNNN and NNN proximate framework Al atoms. Colored regions reflect a Ga^{3+} structure that has the lowest free energy of formation from $[Ga(OH)_2]^+-H^+$ cation pairs at a given temperature (T) and hydrogen partial pressure (P_{H_2}) and water partial pressure (P_{H_2O}) of 10 Pa. The H_2O partial pressure used for this diagram is representative of conditions prevalent during H_2-TPR and NH_3-TPD.

DOI: 10.1021/acscatal.8b01254
ACS Catal. 2018, 8, 6106−6126

formation. Phase diagrams were generated for Ga^{3+} structures at proximate cation-exchange sites associated with both NNN and NNNN pairs of framework Al atoms in order to assess the effect of framework Al−Al interatomic distance on the stability of Ga^{3+} species. Figure 9 shows the phase diagrams for stability of Ga^{3+} species at temperatures between 473 and 823 K, at H_2 partial pressures ranging between 10^{-1} and 10^6 Pa, and for a fixed H_2O partial pressure of 10 Pa. Phase diagrams for additional H_2O partial pressures are included in Figures S.10 and S.11. As seen in Figure 9, at an H_2O partial pressure of 10 Pa and for all temperatures, $[Ga(OH)_2]^+$−H^+ cation pairs are the most favorable structure on proximate cation-exchange sites associated with NNNN pairs of framework Al atoms when Ga/H-MFI is in the oxidized state (H_2 partial pressure <10^2 Pa). When the interatomic Al−Al distance is lowered to ≤5 Å for NNN pairs of framework Al atoms in Figure 9, $[Ga(OH)_2]^+$−H^+ cation pairs are stable only for temperatures <623 K under oxidizing conditions. Above this temperature, the phase diagram predicts that $[Ga(OH)_2]^+$−H^+ cation pairs would undergo intrapair condensation to form $[Ga(OH)]^{2+}$ cations. These findings are in agreement with experimental observations discussed earlier.

Upon reaction between $[Ga(OH)_2]^+$−H^+ cation pairs and H_2 (>10^2 Pa) and in the presence of 10 Pa H_2O, the phase diagram in Figure 9 indicates that the conversion of $[Ga(OH)_2]^+$−H^+ cation pairs at NNNN cation-exchange sites into $[Ga(OH)H]^+$−H^+ pairs is highly favorable thermodynamically. $[Ga(OH)H]^+$−H^+ pairs are the most stable structure throughout the temperature range examined (473−823 K) and at H_2 partial pressures as high as 10^5 Pa. At H_2 pressures >10^5 Pa and temperatures >673 K (and a fixed H_2O partial pressure of 10 Pa), Figure 9 shows that $[Ga(OH)H]^+$−H^+ cation pairs on NNNN cation-exchange sites may further reduce to $[GaH_2]^+$−H^+ pairs. These stability trends also appear to be a strong function of H_2O partial pressure. Under conditions with lower H_2O partial pressure (10^{-1} Pa), the phase diagram for NNNN cation-exchange sites (Figure S.10) predicts that the $[Ga(OH)H]^+$−H^+ cation pairs would form $[GaH_2]^+$−H^+ cation pairs at H_2 partial pressures as low as 3×10^3 Pa and temperatures >700 K. On the other hand, for H_2 pressures lower than 3×10^3 Pa and at temperatures higher than 700 K, $[Ga(OH)H]^+$−H^+ cation pairs would undergo intrapair condensation to form $[GaH]^{2+}$ cations.

For Ga^{3+} structures at NNN cation-exchange sites, the phase diagram in Figure 9 predicts that, at temperatures <623 K and H_2 partial pressures >10^2 Pa (and fixed H_2O partial pressure 10 Pa), $[Ga(OH)_2]^+$−H^+ cation pairs at NNN cation-exchange sites would also form $[Ga(OH)H]^+$−H^+ cation pairs. At temperatures >623 K, these structures would convert into $[GaH]^{2+}$ cations. $[GaH]^{2+}$ cations at NNN proximate cation-exchange sites appear to be stable and resistant to the formation of $[GaH_2]^+$−H^+ cation pairs at all H_2 partial pressures tested. Even at very low H_2O partial pressures (10^{-1} Pa), $[GaH]^{2+}$ cations are still the most thermodynamically stable structure in the presence of H_2 (see Figure S.11).

Further evidence for the presence of GaH_x cations was obtained from in situ infrared spectra of Ga/H-MFI samples, taken at 473 K, after treating Ga/H-MFI samples in 2.5% H_2/He for 1 h at 823 K. Spectra of all three Ga/H-MFI samples (Ga/Al = 0.2, 0.3, 0.5) are shown in Figure 10. Two bands are observed at approximately 2040 and 2060 cm^{-1}, that are absent in the infrared spectra of oxidized Ga/H-MFI samples. In order to assign these vibrational modes to specific GaH_x structures,

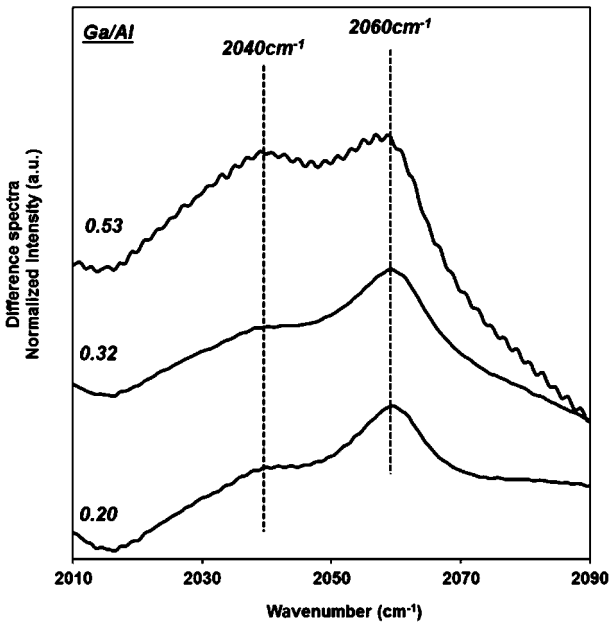

Figure 10. In situ infrared "difference" spectra of Ga/H-MFI samples at 473 K, after treatment in 2.5% H_2/He at 823 K for 1 h. "Difference" spectra were obtained by subtracting the infrared spectra of H-MFI at 473 K from the normalized infrared spectra of Ga/H-MFI at 473 K. All spectra were normalized to the framework Si−O−Si overtone bands between 1900 and 2100 cm^{-1}. Dotted lines show Ga−H vibrational modes.

we examined Ga−H vibrational frequencies computed from QM/MM calculations, for $[GaH]^{2+}$ cations, $[Ga(OH)H]^+$−H^+ cation pairs, and $[GaH_2]^+$−H^+ cation pairs. The predicted frequency for Ga−H stretches in $[GaH]^{2+}$ cations is 2059 cm^{-1} while, for $[Ga(OH)H]^+$−H^+ cation pairs, the predicted Ga−H stretching frequency is 2109 cm^{-1}. For $[GaH_2]^+$ cations (likely present as $[GaH_2]^+$−H^+ cation pairs), the symmetric and asymmetric Ga−H stretching frequencies are predicted to be 2003 and 2043 cm^{-1}, respectively. We, therefore, assign the band at 2060 cm^{-1} in the infrared spectra of Ga/H-MFI to Ga−H stretching vibrations in $[GaH]^{2+}$ cations. We also assign the experimentally observed band at 2040 cm^{-1} to asymmetric Ga−H stretching vibrations in $[GaH_2]^+$ cations. These assignments are consistent with previous observations of GaH_x species in the infrared spectra of H_2 treated Ga/H-MFI.[52] We were unable to observe the Ga−H stretching frequency predicted for $[Ga(OH)H]^+$−H^+ cation pairs in our spectra, likely because of low H_2O partial pressures prevalent in our transmission infrared pellets (∼30 mg sample). Low H_2O concentrations (∼10^{-1} Pa) may enable $[Ga(OH)H]^+$−H^+ cation pairs to reduce to $[GaH_2]^+$−H^+ cation pairs, as predicted by our theoretical calculations. It should also be noted that the relative intensity of the 2040 cm^{-1} band in Figure 10 increases as a function of Ga/Al, consistent with the presence of a higher concentration of $[Ga(OH)H]^+$−H^+ cation pairs or $[GaH_2]^+$−H^+ cation pairs with increasing Ga content.

Additional information about the structures of Ga^{3+} cations in H_2-treated Ga/H-MFI was obtained from the XANES portion of X-ray absorption spectroscopy measurements conducted on H_2-treated Ga/H-MFI samples. As reported in prior studies,[10,12,75,78] we observe that, upon heating Ga/H-MFI in H_2, the XANES absorption maximum shifts from 10 376.6 eV for oxidized Ga/H-MFI to approximately 10 372 eV for Ga/H-MFI, H_2-treated at 823 K, as seen in Figure 11a

DOI: 10.1021/acscatal.8b01254
ACS Catal. 2018, 8, 6106−6126

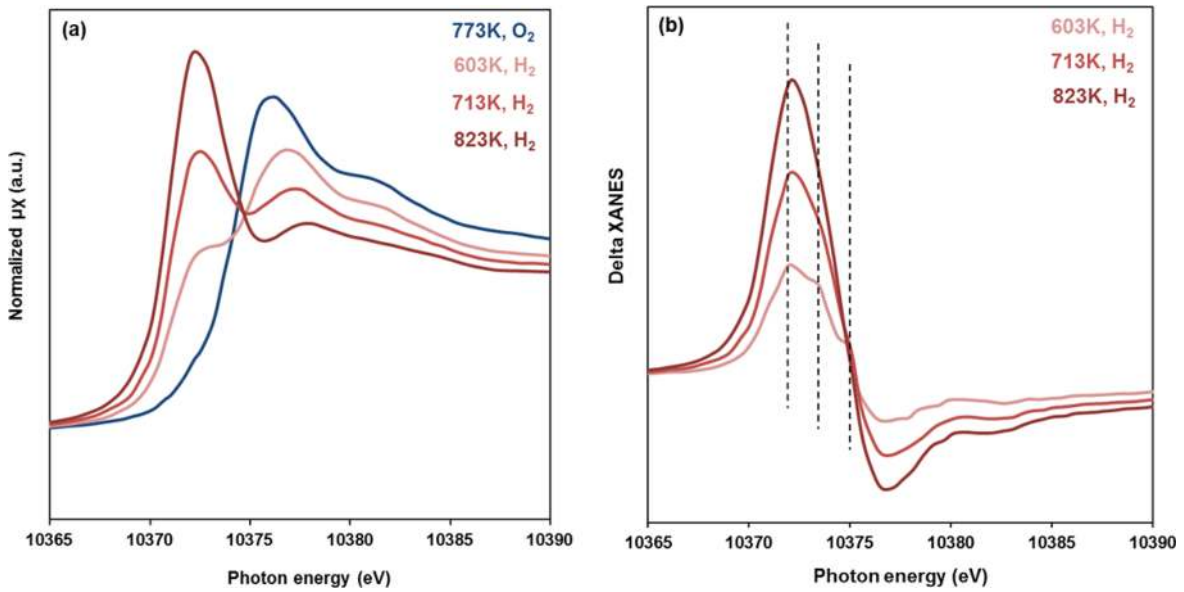

Figure 11. (a) Ga K-edge XANES spectra of H_2-treated Ga/H-MFI (Ga/Al = 0.3) at various temperatures during heating of oxidized Ga/H-MFI in 3% H_2/He. (b) Difference (or Delta) XANES spectra of H_2-treated Ga/H-MFI (Ga/Al = 0.3) obtained by subtracting the XANES spectrum for oxidized Ga/H-MFI from the XANES spectrum of H_2-treated Ga/H-MFI at 603, 713, and 823 K. Dotted lines in delta XANES plot indicate positions of features at 10 375.1, 10 373.6, and 10 372 eV.

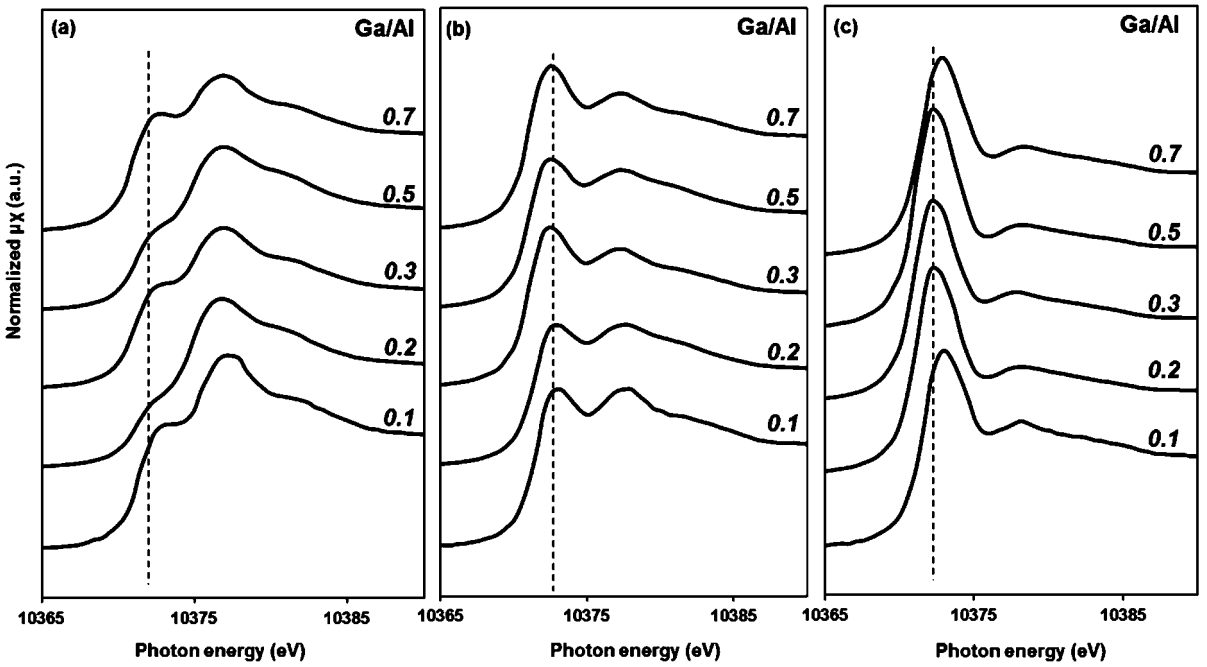

Figure 12. Ga K-edge XANES spectra of H_2-treated Ga/H-MFI (Ga/Al = 0.1 to 0.7) after heating oxidized Ga/H-MFI in 3% H_2/He at (a) 603 K, (b) 713 K, and (c) 823 K. Spectra were collected after 1 h of H_2 treatment at each temperature. Dotted lines show positions of absorption maxima.

for the Ga/Al = 0.3 sample. An increase in temperature from 603 to 823 K during treatment in H_2 results in an increase in the intensity of the lower energy absorption edge (~10 372 eV).

Previous XANES studies of reduced Ga/H-MFI have attributed the feature at 10 372 eV to the presence of Ga^+.[10,12,21] This interpretation has been brought into question by the recent work of Getsoian et al., who examined the effects of Ga coordination and ligation on Ga K-edge XANES spectra.[78] XANES spectra of Ga^{3+} organometallic compounds in which the coordination and identity of Ga-bound ligands was varied systematically revealed that, for every O ligand in a 4-coordinate Ga^{3+} compound, replaced by a less electronegative, more strongly σ-donating H (hydride) or R (alkyl) ligand, the XANES absorption maximum (and edge energy) decreased by approximately 1.5 eV. In addition, when the coordination number around Ga^{3+} decreased from a 4 to 3, an additional 1.5 eV decrease in the XANES absorption maximum occurred.[78] On the basis of these data, it was proposed that 3-coordinate $[GaH_2]^+$ cations form upon H_2 treatment of Ga/H-BEA.[78]

We can predict the XANES absorption maximum (or edge energy) for different GaH_x species in H_2-treated Ga/H-MFI,

DOI: 10.1021/acscatal.8b01254
ACS Catal. 2018, 8, 6106−6126

using the guidelines developed by Getsoian et al.[78] For $[Ga(OH)]^{2+}$ and $[Ga(OH)_2]^{+}-H^{+}$ cation pairs, which have a XANES absorption maximum at 10 376.6 eV, H_2 reduction of these species to 4-coordinate $[Ga(OH)H]^{+}$ cations is expected to decrease the position of the absorption maximum by ~1.5 eV to 10 375.1 eV. The conversion of $[Ga(OH)H]^{+}-H^{+}$ cation pairs to form 4-coordinate $[GaH]^{2+}$ cations is not expected to affect the XANES absorption maximum since both structures have 3 O ligands and 1 H ligand. Further reduction of both species ($[Ga(OH)H]^{+}$ and $[GaH]^{2+}$ cations) to 4-coordinate $[GaH_2]^{+}$ cations is expected to decrease the position of the XANES absorption maximum by another 1.5 eV to about 10 373.6 eV. As proposed by Getsoian et al., the weakened Lewis acidity of Ga^{3+} in 4-coordinate $[GaH_2]^{+}$ cations may result in the loss of the dative $Ga-O_f$ bond at high temperatures, to form 3-coordinate $[GaH_2]^{+}$ cations, possessing only one framework $Ga-O_f$ bond.[78] Such a conversion would further lower the XANES absorption maximum by 1.5 eV to about 10 372.1 eV. Our XANES measurements presented in Figure 11a for the Ga/Al = 0.3 sample (XANES spectra for other Ga/Al ratios are given in Figure 12a–c) show a decrease in the energy of the absorption maximum from 10 376.6 eV for oxidized Ga/H-MFI to about 10 372 eV upon reduction in H_2 at 823 K (a ~4.6 eV decrease), consistent with the presence of 3-coordinate $[GaH_2]^{+}$ cations in H_2-treated samples.

Figure 11b shows the difference XANES spectra for the Ga/Al = 0.3 sample, at various temperatures during treatment in H_2 from ambient temperatures to 823 K. Difference XANES spectra were obtained by subtracting the spectrum of oxidized Ga/H-MFI at 773 K from the spectrum of H_2-treated Ga/H-MFI. Upon heating oxidized Ga/H-MFI in H_2 to 603 K, the difference XANES spectra show the emergence of three features at 10 375.1, 10 373.5, and 10 372 eV that are lower in energy than the absorption maximum for oxidized Ga/H-MFI (10 376.6 eV). On the basis of the preceding discussion, the feature at 10 375.1 eV may reflect either 4-coordinate $[Ga(OH)H]^{+}-H^{+}$ cation pairs or 4-coordinate $[GaH]^{2+}$ cations. On this basis, we assign the feature at 10 373.5 eV to 4-coordinate $[GaH_2]^{+}-H^{+}$ cation pairs and the lowest energy feature to 3-coordinate $[GaH_2]^{+}-H^{+}$ cation pairs. As seen in Figure 11b, we observed that, upon heating samples in H_2 from 603 to 713 K and finally to 823 K, the feature at 10 372 eV increases in intensity and becomes the dominant feature in the difference XANES spectrum at 823 K. The spectrum continues to evolve even as samples are heated past the peak temperature in the H_2-TPR response (~723 K), suggesting that the feature at 10 372 eV is not likely to be due to a Ga^{3+} species that is further reduced than 4-coordinate $[GaH_2]^{+}$ cations but rather due to a Ga^{3+} species with a lower coordination to framework O atoms. The spectrum in Figure 11b suggests that 3-coordinate $[GaH_2]^{+}$ cations form in increasing concentration with increasing temperature.

As seen in Figure 12a–c, a similar increase in the intensity of the absorption maximum at 10 372 eV with an increase in temperature was observed in XANES spectra of other H_2-treated samples of Ga/H-MFI (Ga/Al = 0.1, 0.2, 0.5, and 0.7) suggesting that 3-coordinate $[GaH_2]^{+}$ cations may be present at all Ga/Al ratios. On the basis of our previous characterization, which showed that $[GaH]^{2+}$ cations form in greater concentration at low Ga/Al ratios, we propose that the observed similarity in the absorption maxima (10 372 eV), regardless of Ga/Al ratio, is likely a result of a higher absorption intensity of 3-coordinate $[GaH_2]^{+}$ cations in comparison to 4-coordinate $[GaH]^{2+}$ or $[GaH_2]^{+}$ cations.

A decrease in Ga^{3+} coordination from 4 to 3 corresponds to a change in hybridization around the metal center from sp^3 to sp^2. Consequently, the Ga $4p_z$ orbital becomes nonbonding in 3-coordinate Ga^{3+} structures. In a similar manner to what has been shown for XANES of low-coordinated Zn^{2+} compounds,[79] the allowed photoelectron excitation of a Ga 1s electron into the nonbonding Ga $4p_z$ orbital would result in a stronger absorption at the Ga K-edge than for a similar 1s electron excitation into bonding 4p orbitals. Therefore, even if 3-coordinate $[GaH_2]^{+}$ cations were present at a lower concentration relative to 4-coordinate $[GaH]^{2+}$ cations at low Ga/Al ratios, these species would be expected to dominate the XANES absorption edge. We also note that the absorption maximum at 823 K for the Ga/Al = 0.1 sample (~10 373 eV) seen in Figure 12c is about 1 eV higher than the absorption maxima for the samples with Ga/Al = 0.2 and Ga/Al = 0.3 (~10 372 eV). The presence of $[GaH]^{2+}$ cations (with an absorption maximum of ~10 375 eV), in coexistence with some 3-coordinate $[GaH_2]^{+}$ cations (with an absorption maximum of ~10 372 eV) at low Ga/Al ratios, may be responsible for this observation. The EXAFS spectra of H_2-treated Ga/H-MFI, when fit to a 2 shell Ga–O model, showed a total decrease in Ga–O coordination from 4 in oxidized Ga/H-MFI to between 2 and 3 in Ga/H-MFI treated in H_2 at 723 K (see Text S.8 and Table 4). Due to the weak photoelectron scattering from H atoms,[80] the observed decrease in Ga–O coordination is consistent with the replacement of Ga-bound OH ligands with H ligands. We could not perform a more detailed analysis of the EXAFS spectra of H_2-treated Ga/H-MFI due to the coexistence of multiple Ga species.

4. CONCLUSIONS

Ga/H-MFI with Ga/Al ratios ranging from 0.1 to 0.7 was synthesized via the vapor-phase reaction of dehydrated H-MFI with $GaCl_3$. This process results in the exchange of Brønsted acid O–H groups by monovalent $[GaCl_2]^{+}$ cations. The maximum level of cation exchange achievable by this means is $[GaCl_2]^{+}/Al_{tot}$ ~0.7. H_2 reduction at 823 K of the as-exchanged zeolites results in the stoichiometric removal of Ga-bound Cl as HCl and the formation of $[GaH_2]^{+}$ cations. Upon O_2 oxidation at 773 K, these structures form oxidized Ga^{3+} species; however, crystalline β-Ga_2O_3 is not detectable by Raman spectroscopy. For Ga/Al = 0.1, about half of the $[GaH_2]^{+}$ cations are oxidized to divalent $[Ga(OH)]^{2+}$ cations, bound to proximate cation-exchange sites associated with pairs of framework Al atoms located ≤5 Å apart, whereas the remainder $[GaH_2]^{+}$ cations are oxidized to $[Ga(OH)_2]^{+}-H^{+}$ cation pairs bound to proximate cation-exchange sites associated with pairs of framework Al atoms located >5 Å apart. For Ga/Al ratios above 0.1 but below 0.3, an increasing fraction of the cation-exchanged Ga^{3+} is present as $[Ga(OH)_2]^{+}-H^{+}$ cation pairs bound to proximate cation-exchange sites. For Ga/Al ratios higher than 0.3, wavelet analysis of EXAFS data shows that neutral GaO_x species, not associated with cation-exchange sites, are formed. Upon H_2 reduction of oxidized Ga/H-MFI, $[Ga(OH)]^{2+}$ cations and $[Ga(OH)_2]^{+}-H^{+}$ cation pairs form $[GaH]^{2+}$ cations at low Ga/Al ratios (~0.1) and $[Ga(OH)H]^{+}-H^{+}$ cation pairs for Ga/Al ≤ 0.3. Phase diagrams calculated to assess the thermodynamic stability of species formed upon H_2 reduction of $[Ga(OH)_2]^{+}-H^{+}$ cation pairs indicate that $[GaH]^{2+}$ cations are more stable at proximate cation-exchange sites with framework Al–Al

DOI: 10.1021/acscatal.8b01254
ACS Catal. 2018, 8, 6106–6126

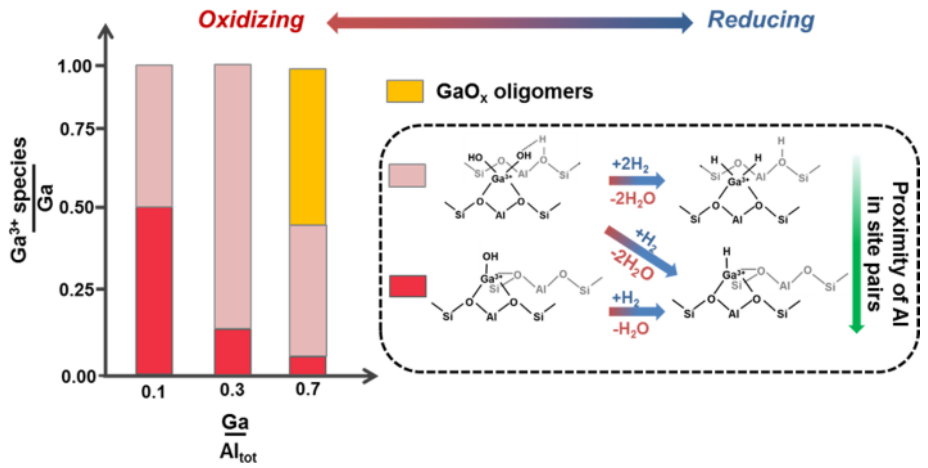

Figure 13. Ga^{3+} speciation in Ga/H-MFI under oxidizing conditions (red) and reducing conditions (blue).

interatomic distances ≤5 Å, while for proximate cation-exchange sites with framework Al−Al interatomic distances >5 Å, $[Ga(OH)H]^+-H^+$ cation pairs are more likely to form when H_2 reduction is carried out with a background H_2O partial pressure of 10 Pa. For lower partial pressures of H_2O (10^{-1} Pa), the calculated phase diagrams predict that $[Ga(OH)H]^+-H^+$ cation pairs associated with NNNN framework Al atoms further reduce to $[GaH_2]^+-H^+$ cation pairs. Evidence for $[GaH]^{2+}$ cations and $[GaH_2]^+-H^+$ cation pairs was obtained via infrared spectroscopy under reducing conditions. For temperatures above 713 K, XANES data suggests that 4-coordinate $[GaH_2]^+$ cations transform to 3-coordinate $[GaH_2]^+$ cations. The preferential formation of $[GaH]^{2+}$ cations at low Ga/Al ratios (~0.1) is a consequence of the thermodynamic preference for these cations to locate at cation-exchange sites associated with framework Al atoms that are ≤5 Å apart. A summary of how Ga^{3+} speciation changes with Ga/Al ratio in both the oxidized and reduced forms of Ga/H-MFI is shown in Figure 13. The present study provides essential information for understanding the structure of reduced Ga^{3+} species as active centers for the dehydrogenation and dehydrocyclization of light alkanes to alkenes and aromatics.

■ ASSOCIATED CONTENT

Supporting Information

The Supporting Information is available free of charge on the ACS Publications website at DOI: 10.1021/acscatal.8b01254.

Details regarding material synthesis, characterization, and theoretical calculations (PDF)

■ AUTHOR INFORMATION

Corresponding Author

*E-mail: alexbell@berkeley.edu.

ORCID

Jeroen Van der Mynsbrugge: 0000-0003-3852-4726
Martin Head-Gordon: 0000-0002-4309-6669
Alexis T. Bell: 0000-0002-5738-4645

Notes

The authors declare no competing financial interest.

■ ACKNOWLEDGMENTS

This work was supported by Chevron Energy Technology Company. Computational resources were provided by UC Berkeley's Molecular Graphics and Computation Facility (supported by NIH S10OD023532). We would like to thank James Dombrowski and Sam Wood for assistance with development of synthetic protocols and Christopher Ho for helpful technical discussions. E.M. gratefully acknowledges support from the Abu Dhabi National Oil Company in the form of a fellowship. We also thank Dr. Ping Yu (UC-Davis) for assistance with NMR measurements. This research used resources of the Advanced Photon Source, a U.S. Department of Energy (DOE) Office of Science User Facility operated for the DOE Office of Science by Argonne National Laboratory under Contract No. DE-AC02-06CH11357. XAS measurements were conducted at Beamline 5BMD at the Advanced Photon Source (APS), Argonne National Laboratory. We thank Dr. Qing Ma (Advanced Photon Source, ANL) and Prof. Jeffrey Miller (Purdue University) for assistance with XAS measurements.

■ REFERENCES

(1) Siirola, J. J. The Impact of Shale Gas in the Chemical Industry. *AIChE J.* **2014**, *60*, 810−819.
(2) Sattler, J. J. H. B.; Ruiz-Martinez, J.; Santillan-Jimenez, E.; Weckhuysen, B. M. Catalytic Dehydrogenation of Light Alkanes on Metals and Metal Oxides. *Chem. Rev.* **2014**, *114*, 10613−10653.
(3) Gnep, N. S.; Doyemet, J. Y.; Seco, A. M.; Ribeiro, F. R.; Guisnet, M. Conversion of Light Alkanes into Aromatic Hydrocarbons: 1-Dehydrocyclodimerization of Propane on PtHZSM-5 Catalysts. *Appl. Catal.* **1987**, *35*, 93−108.
(4) Biscardi, J. A.; Iglesia, E. Structure and Function of Metal Cations in Light Alkane Reactions Catalyzed by Modified H-ZSM5. *Catal. Today* **1996**, *31*, 207−231.
(5) Biscardi, J. A.; Meitzner, G. D.; Iglesia, E. Structure and Density of Active Zn Species in Zn/H-ZSM5 Propane Aromatization Catalysts. *J. Catal.* **1998**, *179*, 192−202.
(6) Li, W.; Yu, S. Y.; Meitzner, G. D.; Iglesia, E. Structure and Properties of Cobalt-Exchanged H-ZSM5 Catalysts for Dehydrogenation and Dehydrocyclization of Alkanes. *J. Phys. Chem. B* **2001**, *105*, 1176−1184.
(7) Seddon, D. Paraffin Oligomerisation to Aromatics. Catal. *Catal. Today* **1990**, *6*, 351−372.
(8) Chen, N. Y.; Yan, T. Y. M2 Forming-A Process for Aromatization of Light Hydrocarbons. *Ind. Eng. Chem. Process Des. Dev.* **1986**, *25*, 151−155.

DOI: 10.1021/acscatal.8b01254
ACS Catal. 2018, 8, 6106−6126

(9) Anderson, R. F.; Johnson, J. A.; Mowry, J. R. Cyclar: One Step Processing of LPG to Aromatics and Hydrogen. In *American Institute of Chemical Engineers Spring National Meeting*, Houston, TX, 1985.
(10) Meitzner, G. D.; Iglesia, E.; Baumgartner, J. E.; Huang, E. S. The Chemical State of Gallium in Working Alkane Dehydrocyclodimerization Catalysts. In Situ Gallium K-Edge X-Ray Absorption Spectroscopy. *J. Catal.* **1993**, *140*, 209−225.
(11) Krishnamurthy, G.; Bhan, A.; Delgass, W. N. Identity and Chemical Function of Gallium Species Inferred from Microkinetic Modeling Studies of Propane Aromatization over Ga/HZSM-5 Catalysts. *J. Catal.* **2010**, *271*, 370−385.
(12) Hensen, E. J. M.; García-Sánchez, M.; Rane, N.; Magusin, P. C. M. M.; Liu, P. H.; Chao, K. J.; Van Santen, R. A. In Situ Ga K Edge XANES Study of the Activation of Ga/ZSM-5 Prepared by Chemical Vapor Deposition of Trimethylgallium. Catal. *Catal. Lett.* **2005**, *101*, 79−85.
(13) Kazansky, V. B.; Subbotina, I. R.; Van Santen, R. A.; Hensen, E. J. M. DRIFTS Study of the Nature and Chemical Reactivity of Gallium Ions in Ga/ZSM-5: II. Oxidation of Reduced Ga Species in ZSM-5 by Nitrous Oxide or Water. *J. Catal.* **2005**, *233*, 351−358.
(14) Price, G. L.; Kanazirev, V. Ga_2O_3/HZSM-5 Propane Aromatization Catalysts: Formation of Active Centers via Solid-State Reaction. *J. Catal.* **1990**, *126*, 267−278.
(15) Kwak, B.; Sachtler, W. Effect of Ga/Proton Balance in Ga/HZSM-5 Catalysts on C_3 Conversion to Aromatics. *J. Catal.* **1994**, *145*, 456−463.
(16) Frash, M. V.; van Santen, R. A. Activation of Small Alkanes in Ga-Exchanged Zeolites: A Quantum Chemical Study of Ethane Dehydrogenation. *J. Phys. Chem. A* **2000**, *104*, 2468−2475.
(17) Hensen, E. J. M.; Pidko, E. A.; Rane, N.; Van Santen, R. A. Water-Promoted Hydrocarbon Activation Catalyzed by Binuclear Gallium Sites in ZSM-5 Zeolite. *Angew. Chem., Int. Ed.* **2007**, *46*, 7273−7276.
(18) Rane, N.; Kersbulck, M.; van Santen, R. A.; Hensen, E. J. M. Cracking of N-Heptane over Brønsted Acid Sites and Lewis Acid Ga Sites in ZSM-5 Zeolite. *Microporous Mesoporous Mater.* **2008**, *110*, 279−291.
(19) Rodrigues, V. de O.; Eon, J. G.; Faro, A. C. Correlations between Dispersion, Acidity, Reducibility, and Propane Aromatization Activity of Gallium Species Supported on HZSM5 Zeolites. *J. Phys. Chem. C* **2010**, *114*, 4557−4567.
(20) Meriaudeau, P.; Naccache, C. H-ZSM-5 Supported Ga_2O_3 Dehydrocyclisation Catalysts Infrared Spectroscopic Evidence of Gallium Oxide Surface Mobility. *Appl. Catal.* **1991**, *73*, L13−L18.
(21) Schreiber, M. W.; Plaisance, C. P.; Baumgärtl, M.; Reuter, K.; Jentys, A.; Bermejo-Deval, R.; Lercher, J. A. Lewis-Brønsted Acid Pairs in Ga/H-ZSM-5 to Catalyze Dehydrogenation of Light Alkanes. *J. Am. Chem. Soc.* **2018**, *140*, 4849−4859.
(22) Joly, J. F.; Ajot, H.; Merlen, E.; Raatz, F.; Alario, F. Parameters Affecting the Dispersion of the Gallium Phase of Gallium H-MFI Aromatization Catalysts. *Appl. Catal., A* **1991**, *79*, 249−263.
(23) Nowak, I.; Quartararo, J.; Derouane, E. G.; Védrine, J. C. Effect of H_2-O_2 Pre-Treatments on the State of Gallium in Ga/H-ZSM-5 Propane Aromatisation Catalysts. *Appl. Catal., A* **2003**, *251*, 107−120.
(24) Abdul Hamid, S. B.; Derouane, E.; Mériaudeau, P.; Naccache, C. Effect of Reductive and Oxidative Atmospheres on the Propane Aromatisation Activity and Selectivity of Ga/H-ZSM-5 Catalysts. Catal. *Catal. Today* **1996**, *31*, 327−334.
(25) Bhan, A.; Nicholas Delgass, W. Propane Aromatization over HZSM-5 and Ga/HZSM-5 Catalysts. *Catal. Rev.: Sci. Eng.* **2008**, *50*, 19−151.
(26) Rane, N.; Overweg, A. R.; Kazansky, V. B.; van Santen, R. A.; Hensen, E. J. M. Characterization and Reactivity of Ga^+ and GaO^+ Cations in Zeolite ZSM-5. *J. Catal.* **2006**, *239*, 478−485.
(27) Janda, A.; Bell, A. T. Effects of Si/Al Ratio on the Distribution of Framework Al and on the Rates of Alkane Monomolecular Cracking and Dehydrogenation in H-MFI. *J. Am. Chem. Soc.* **2013**, *135*, 19193−19207.
(28) Yoder, L. Adaptation of the Mohr Volumetric Method to General Determinations of Chlorine. *J. Ind. Eng. Chem.* **1919**, *11*, 755.
(29) Signorile, M.; Bonino, F.; Damin, A.; Bordiga, S. UV-Raman Fingerprint of Brønsted Sites in MFI Zeolites: A Useful Marker in Dealumination Detection. *J. Phys. Chem. C* **2016**, *120*, 18088−18092.
(30) Engelhardt, G.; Lohse, U.; Lippmaa, E.; Tarmak, M.; Magi, M. ^{29}Si-NMR-Untersuchungen Zur Verteilung Der Silicium Und Aluminiumatome Im Alumosilicatgitter von Zeolithen Mit Faujasit-Struktur.r. *Z. Anorg. Allg. Chem.* **1981**, *482*, 49−64.
(31) Kentgens, A. P. M.; Scholle, J.; Veeman, W. S. Effect of Hydration on the Local Symmetry around Aluminum in ZSM-5 Zeolites Studied by Aluminum-27 Nuclear Magnetic Resonance. *J. Phys. Chem.* **1983**, *87*, 4357−4360.
(32) Ravel, B.; Newville, M. ATHENA, ARTEMIS, HEPHAESTUS: Data Analysis for X-Ray Absorption Spectroscopy Using IFEFFIT. *J. Synchrotron Radiat.* **2005**, *12*, 537−541.
(33) Deiseroth, V. H. J.; Muller-buschbaum, H. K. Uber Erdalkalimetalloxogallate. 111 Untersuchung Des Aufbaus von $CaGa_2O_4$. *Z. Anorg. Allg. Chem.* **1973**, *396*, 157−164.
(34) Funke, H.; Scheinost, A. C.; Chukalina, M. Wavelet Analysis of Extended X-Ray Absorption Fine Structure Data. *Phys. Rev. B: Condens. Matter Mater. Phys.* **2005**, *71*, 94110.
(35) Zimmerman, P. M.; Head-Gordon, M.; Bell, A. T. Selection and Validation of Charge and Lennard-Jones Parameters for QM/MM Simulations of Hydrocarbon Interactions with Zeolites. *J. Chem. Theory Comput.* **2011**, *7*, 1695−1703.
(36) Li, Y.-P.; Gomes, J.; Mallikarjun Sharada, S.; Bell, A. T.; Head-Gordon, M. Improved Force-Field Parameters for QM/MM Simulations of the Energies of Adsorption for Molecules in Zeolites and a Free Rotor Correction to the Rigid Rotor Harmonic Oscillator Model for Adsorption Enthalpies. *J. Phys. Chem. C* **2015**, *119*, 1840−1850.
(37) Chai, J.-D.; Head-Gordon, M. Systematic Optimization of Long-Range Corrected Hybrid Density Functionals. *J. Chem. Phys.* **2008**, *128*, 84106.
(38) Chai, J.-D.; Head-Gordon, M. Long-Range Corrected Hybrid Density Functionals with Damped Atom−atom Dispersion Corrections. *Phys. Chem. Chem. Phys.* **2008**, *10*, 6615.
(39) Swisher, J. A.; Hansen, N.; Maesen, T.; Keil, F. J.; Smit, B.; Bell, A. T. Theoretical Simulation of N-Alkane Cracking on Zeolites. *J. Phys. Chem. C* **2010**, *114*, 10229−10239.
(40) Mallikarjun Sharada, S.; Zimmerman, P. M.; Bell, A. T.; Head-Gordon, M. Insights into the Kinetics of Cracking and Dehydrogenation Reactions of Light Alkanes in H-MFI. *J. Phys. Chem. C* **2013**, *117*, 12600−12611.
(41) Gomes, J.; Zimmerman, P. M.; Head-Gordon, M.; Bell, A. T. Accurate Prediction of Hydrocarbon Interactions with Zeolites Utilizing Improved Exchange-Correlation Functionals and QM/MM Methods: Benchmark Calculations of Adsorption Enthalpies and Application to Ethene Methylation by Methanol. *J. Phys. Chem. C* **2012**, *116*, 15406−15414.
(42) Van Speybroeck, V.; Van der Mynsbrugge, J.; Vandichel, M.; Hemelsoet, K.; Lesthaeghe, D.; Ghysels, A.; Marin, G. B.; Waroquier, M. First Principle Kinetic Studies of Zeolite-Catalyzed Methylation Reactions. *J. Am. Chem. Soc.* **2011**, *133*, 888−899.
(43) Van der Mynsbrugge, J.; Hemelsoet, K.; Vandichel, M.; Waroquier, M.; Van Speybroeck, V. Efficient Approach for the Computational Study of Alcohol and Nitrile Adsorption in H-ZSM-5. *J. Phys. Chem. C* **2012**, *116*, 5499−5508.
(44) Van der Mynsbrugge, J.; Visur, M.; Olsbye, U.; Beato, P.; Bjørgen, M.; Van Speybroeck, V.; Svelle, S. Methylation of Benzene by Methanol: Single-Site Kinetics over H-ZSM-5 and H-Beta Zeolite Catalysts. *J. Catal.* **2012**, *292*, 201−212.
(45) Van der Mynsbrugge, J.; Janda, A.; Mallikarjun Sharada, S.; Lin, L.-C.; Van Speybroeck, V.; Head-Gordon, M.; Bell, A. T. Theoretical Analysis of the Influence of Pore Geometry on Monomolecular Cracking and Dehydrogenation of N-Butane in Brønsted-Acid Zeolites. *ACS Catal.* **2017**, *7*, 2685−2697.

DOI: 10.1021/acscatal.8b01254
ACS Catal. 2018, 8, 6106−6126

(46) Joshi, Y. V.; Thomson, K. T. High Ethane Dehydrogenation Activity of $[GaH]^{2+}$ Al Pair Sites in Ga/H-[Al]ZSM-5: A DFT Thermochemical Analysis of the Catalytic Sites under Reaction Conditions. *J. Catal.* **2007**, *246*, 249−265.
(47) Verstraelen, T.; Van Speybroeck, V.; Waroquier, M. ZEOBUILDER: A GUI Toolkit for the Construction of Complex Molecular Structures on the Nanoscale with Building Blocks. *J. Chem. Inf. Model.* **2008**, *48*, 1530−1541.
(48) Shao, Y.; Gan, Z.; Epifanovsky, E.; Gilbert, A. T. B.; Wormit, M.; Kussmann, J.; Lange, A. W.; Behn, A.; Deng, J.; Feng, X.; Ghosh, D.; Goldey, M.; Horn, P. R.; Jacobson, L. D.; Kaliman, I.; Khaliullin, R. Z.; Kuś, T.; Landau, A.; Liu, J.; Proynov, E. I.; Rhee, Y. M.; Richard, R. M.; Rohrdanz, M. A.; Steele, R. P.; Sundstrom, E. J.; Woodcock, H. L.; Zimmerman, P. M.; Zuev, D.; Albrecht, B.; Alguire, E.; Austin, B.; Beran, G. J. O.; Bernard, Y. A.; Berquist, E.; Brandhorst, K.; Bravaya, K. B.; Brown, S. T.; Casanova, D.; Chang, C.-M.; Chen, Y.; Chien, S. H.; Closser, K. D.; Crittenden, D. L.; Diedenhofen, M.; DiStasio, R. A.; Do, H.; Dutoi, A. D.; Edgar, R. G.; Fatehi, S.; Fusti-Molnar, L.; Ghysels, A.; Golubeva-Zadorozhnaya, A.; Gomes, J.; Hanson-Heine, M. W. D.; Harbach, P. H. P.; Hauser, A. W.; Hohenstein, E. G.; Holden, Z. C.; Jagau, T.-C.; Ji, H.; Kaduk, B.; Khistyaev, K.; Kim, J.; Kim, J.; King, R. A.; Klunzinger, P.; Kosenkov, D.; Kowalczyk, T.; Krauter, C. M.; Lao, K. U.; Laurent, A. D.; Lawler, K. V.; Levchenko, S. V.; Lin, C. Y.; Liu, F.; Livshits, E.; Lochan, R. C.; Luenser, A.; Manohar, P.; Manzer, S. F.; Mao, S.-P.; Mardirossian, N.; Marenich, A. V.; Maurer, S. A.; Mayhall, N. J.; Neuscamman, E.; Oana, C. M.; Olivares-Amaya, R.; O'Neill, D. P.; Parkhill, J. A.; Perrine, T. M.; Peverati, R.; Prociuk, A.; Rehn, D. R.; Rosta, E.; Russ, N. J.; Sharada, S. M.; Sharma, S.; Small, D. W.; Sodt, A.; Stein, T.; Stück, D.; Su, Y.-C.; Thom, A. J. W.; Tsuchimochi, T.; Vanovschi, V.; Vogt, L.; Vydrov, O.; Wang, T.; Watson, M. A.; Wenzel, J.; White, A.; Williams, C. F.; Yang, J.; Yeganeh, S.; Yost, S. R.; You, Z.-Q.; Zhang, I. Y.; Zhang, X.; Zhao, Y.; Brooks, B. R.; Chan, G. K. L.; Chipman, D. M.; Cramer, C. J.; Goddard, W. A.; Gordon, M. S.; Hehre, W. J.; Klamt, A.; Schaefer, H. F.; Schmidt, M. W.; Sherrill, C. D.; Truhlar, D. G.; Warshel, A.; Xu, X.; Aspuru-Guzik, A.; Baer, R.; Bell, A. T.; Besley, N. A.; Chai, J.-D.; Dreuw, A.; Dunietz, B. D.; Furlani, T. R.; Gwaltney, S. R.; Hsu, C.-P.; Jung, Y.; Kong, J.; Lambrecht, D. S.; Liang, W.; Ochsenfeld, C.; Rassolov, V. A.; Slipchenko, L. V.; Subotnik, J. E.; Van Voorhis, T.; Herbert, J. M.; Krylov, A. I.; Gill, P. M. W.; Head-Gordon, M. Advances in Molecular Quantum Chemistry Contained in the Q-Chem 4 Program Package. *Mol. Phys.* **2015**, *113*, 184−215.
(49) Grimme, S. Supramolecular Binding Thermodynamics by Dispersion-Corrected Density Functional Theory. *Chem. - Eur. J.* **2012**, *18*, 9955−9964.
(50) Brunetti, B.; Piacente, V.; Scardala, P. Vapor Pressures of Gallium Trifluoride, Trichloride, and Triiodide and Their Standard Sublimation Enthalpies. *J. Chem. Eng. Data* **2010**, *55*, 98−102.
(51) Nogai, S.; Schmidbaur, H. Dichlorogallane $(HGaCl_2)_2$: Its Molecular Structure and Synthetic Potential. *Inorg. Chem.* **2002**, *41*, 4770−4774.
(52) Kazansky, V. B.; Subbotina, I. R.; van Santen, R. A.; Hensen, E. J. M. DRIFTS Study of the Chemical State of Modifying Gallium Ions in Reduced Ga/ZSM-5 Prepared by Impregnation. I. Observation of Gallium Hydrides and Application of CO Adsorption as Molecular Probe for Reduced Gallium Ions. *J. Catal.* **2004**, *227*, 263−269.
(53) Collins, S. E.; Baltanás, M. A.; Bonivardi, A. L. Hydrogen Chemisorption on Gallium Oxide Polymorphs. *Langmuir* **2005**, *21*, 962−970.
(54) Vecchietti, J.; Baltanás, M. A.; Gervais, C.; Collins, S. E.; Blanco, G.; Matz, O.; Calatayud, M.; Bonivardi, A. Insights on Hydride Formation over Cerium-Gallium Mixed Oxides: A Mechanistic Study for Efficient H_2 Dissociation. *J. Catal.* **2017**, *345*, 258−269.
(55) Jacobs, P. A.; Von Ballmoos, R. Framework Hydroxyl Groups of H-ZSM-5 Zeolites. *J. Phys. Chem.* **1982**, *86*, 3050−3052.
(56) Woolery, G. L.; Alemany, L. B.; Dessau, R. M.; Chester, A. W. Spectroscopic Evidence for the Presence of Internal Silanols in Highly Siliceous ZSM-5. *Zeolites* **1986**, *6*, 14−16.
(57) Ong, L. H.; Dömök, M.; Olindo, R.; Van Veen, A. C.; Lercher, J. A. Dealumination of HZSM-5 via Steam-Treatment. *Microporous Mesoporous Mater.* **2012**, *164*, 9−20.
(58) Paolucci, C.; Parekh, A. A.; Khurana, I.; Di Iorio, J. R.; Li, H.; Albarracin Caballero, J. D.; Shih, A. J.; Anggara, T.; Delgass, W. N.; Miller, J. T.; Ribeiro, F. H.; Gounder, R.; Schneider, W. F. Catalysis in a Cage: Condition-Dependent Speciation and Dynamics of Exchanged Cu Cations in SSZ-13 Zeolites. *J. Am. Chem. Soc.* **2016**, *138*, 6028−6048.
(59) Klinowski, J.; Thomas, J. M.; Anderson, M. W.; Fyfe, C. A.; Gobbi, G. C. Dealumination of Mordenite Using Silicon Tetrachloride Vapour. *Zeolites* **1983**, *3*, 5−7.
(60) Di Iorio, J. R.; Bates, S. A.; Verma, A. A.; Delgass, W. N.; Ribeiro, F. H.; Miller, J. T.; Gounder, R. The Dynamic Nature of Brønsted Acid Sites in Cu-Zeolites During NO_x Selective Catalytic Reduction: Quantification by Gas-Phase Ammonia Titration. *Top. Catal.* **2015**, *58*, 424−434.
(61) Pokrovski, G. S.; Schott, J.; Hazemann, J.; Farges, F.; Pokrovsky, O. S. An X-Ray Absorption Fine Structure and Nuclear Magnetic Resonance Spectroscopy Study of Gallium−silica Complexes in Aqueous Solution. *Geochim. Cosmochim. Acta* **2002**, *66*, 4203−4222.
(62) Zheng, B.; Hua, W.; Yue, Y.; Gao, Z. Dehydrogenation of Propane to Propene over Different Polymorphs of Gallium Oxide. *J. Catal.* **2005**, *232*, 143−151.
(63) Dymock, K.; Palenik, G. J. Tris(acetylacetonato)gallium(III). *Acta Crystallogr., Sect. B: Struct. Crystallogr. Cryst. Chem.* **1974**, *B30*, 1364−1366.
(64) Teo, B. K. *EXAFS: Basic Principles and Data Analysis (Inorganic Chemistry Concepts)*, 9th ed.; Springer: New York, 1986.
(65) Calvin, S. *XAFS for Everyone*, 1st ed.; CRC Press: Boca Raton, 2013.
(66) Eisenberger, P.; Brown, G. S. The Study of Disordered Systems by EXAFS: Limitations. *Solid State Commun.* **1979**, *29*, 481−484.
(67) Clausen, B. S.; Nørskov, J. K. Asymmetric Pair Distribution Functions in Catalysts. *Top. Catal.* **2000**, *10*, 221−230.
(68) Bus, E.; Miller, J. T.; Kropf, a J.; Prins, R.; van Bokhoven, J. a. Analysis of in Situ EXAFS Data of Supported Metal Catalysts Using the Third and Fourth Cumulant. *Phys. Chem. Chem. Phys.* **2006**, *8*, 3248−3258.
(69) Åhman, J.; Svensson, G.; Albertsson, J. A Reinvestigation of β-Gallium Oxide. *Acta Crystallogr., Sect. C: Cryst. Struct. Commun.* **1996**, *52*, 1336−1338.
(70) Munoz, M.; Argoul, P.; Farges, F. Continuous Cauchy Wavelet Transform Analyses of EXAFS Spectra: A Qualitative Approach. *Am. Mineral.* **2003**, *88*, 694−700.
(71) Muñoz, M.; Farges, F.; Argoul, P. Continuous Cauchy Wavelet Transform of XAFS Spectra. *Phys. Scr.* **2005**, *T115*, 221−222.
(72) Funke, H.; Chukalina, M.; Voegelin, A.; Scheinost, A. C. Improving Resolution in K and R Space: A FEFF-Based Wavelet for EXAFS Data Analysis. *AIP Conf. Proc.* **2006**, *882*, 72−74.
(73) Fleischman, S. D.; Scott, S. L. Evidence for the Pairwise Disposition of Grafting Sites on Highly Dehydroxylated Silicas via Their Reactions with $Ga(CH_3)_3$. *J. Am. Chem. Soc.* **2011**, *133*, 4847−4855.
(74) Searles, K.; Siddiqi, G. G.; Safonova, O. V.; Coperet, C. Silica-Supported Isolated Gallium Sites as Highly Active, Selective and Stable Propane Dehydrogenation Catalysts. *Chem. Sci.* **2017**, *8*, 2661−2666.
(75) Faro, A. C.; Rodrigues, V. D. O.; Eon, J. G. In Situ X-Ray Absorption Study of the Genesis and Nature of the Reduced Gallium Species in Ga/HZSM5 Catalysts. *J. Phys. Chem. C* **2011**, *115*, 4749−4756.
(76) Da Costa, P.; Moden, B.; Meitzner, G. D.; Lee, D. K.; Iglesia, E. Spectroscopic and Chemical Characterization of Active and Inactive Cu Species in NO Decomposition Catalysts Based on Cu-ZSM5. *Phys. Chem. Chem. Phys.* **2002**, *4*, 4590−4601.
(77) Zhang, Y.; Drake, I. J.; Bell, A. T. Characterization of Cu-ZSM-5 Prepared by Solid-State Ion Exchange of H-ZSM-5 with CuCl. *Chem. Mater.* **2006**, *18*, 2347−2356.

DOI: 10.1021/acscatal.8b01254
ACS Catal. 2018, 8, 6106−6126

(78) Getsoian, A. B.; Das, U.; Camacho-Bunquin, J.; Zhang, G.; Gallagher, J. R.; Hu, B.; Cheah, S.; Schaidle, J. A.; Ruddy, D. A.; Hensley, J. E.; Krause, T. R.; Curtiss, L. A.; Miller, J. T.; Hock, A. S. Organometallic Model Complexes Elucidate the Active Gallium Species in Alkane Dehydrogenation Catalysts Based on Ligand Effects in Ga K-Edge XANES. *Catal. Sci. Technol.* **2016**, *6*, 6339−6353.
(79) Camacho-Bunquin, J.; Aich, P.; Ferrandon, M.; Getsoian, A. B.; Das, U.; Dogan, F.; Curtiss, L. A.; Miller, J. T.; Marshall, C. L.; Hock, A. S.; Stair, P. C. Single-Site Zinc on Silica Catalysts for Propylene Hydrogenation and Propane Dehydrogenation: Synthesis and Reactivity Evaluation Using an Integrated Atomic Layer Deposition-Catalysis Instrument. *J. Catal.* **2017**, *345*, 170−182.
(80) Lengeler, B. Lattice Site Location of Hydrogen by Use of Extended X-Ray Absorption Fine Structure. *Phys. Rev. Lett.* **1984**, *53*, 74−77.

DOI: 10.1021/acscatal.8b01254
ACS Catal. 2018, 8, 6106−6126